TITLE:

Abstracts for the Society of Nuclear Medicine and Molecular Imaging, Greater New York and New England Chapters, 36th Annual Northeast Regional Scientific Meeting, Hartford, Connecticut, November, 2023

Title

Intraperitoneal urine leak during early post-renal transplant period: using nuclear medicine renal scan for early detection – a case report.

Yunbeen Bae[1], Erika K. Ekengren[2], Samantha Harrington[2], Merissa Zeman[2], Bashar S. Kako[2], Thomas S.C. Ng[2]

[1]Massachusetts Institute of Technology

[2]Division of Nuclear Medicine and Molecular Imaging, Department of Radiology, Massachusetts General Hospital, Harvard Medical School

Background: Urine leak is a rare but critical surgical complication in the early post-transplant period.[1] Living-donor renal transplants generally have better outcomes from these complications than cadaver-donor recipients, but early detection of urine leak following surgery can result in successful treatment. Ultrasound and CT are used to monitor recently transplanted grafts for prognosis.[2] During this early post-transplant period, CT is obtained without IV contrast to prevent damage to the transplanted kidney. Lack of iodinated contrast makes urine leaks challenging to detect. However, technetium-99m MAG3 renal scans may be useful in this setting. Previously, an extraperitoneal leak after renal transplantation was identified using radionuclide imaging.[3] Our case demonstrates how nuclear medicine imaging can diagnose an intraperitoneal leak during the post-transplant period.

Methods/Results: The patient is a 27-year-old female who received a deceased-donor kidney transplant but showed no urine output despite Foley catheterization. This raised concerns for a renal dysfunction or urine leak, so a CT scan of the abdomen and pelvis without IV contrast was obtained on postoperative day one. On the CT scan, no urine leak was detected, and the renal transplant did not demonstrate hydronephrosis; however, ascites was noted (Figure 1). The lack of hydronephrosis argued against a potential obstruction as the cause of the patient's anuria. Additionally, on the CT the bladder was decompressed, and a urinary catheter was in place. The bladder was noted to be inferior to a prominent collection of ascites in Figure 1. Due to the ongoing decreased urine production, technetium-99m MAG3 renography was performed on post operative Day 2 to further evaluate the renal transplant function. Radionuclide scan revealed prompt renal uptake and timely excretion into a midline collection (Figure 2). Due to the unaddressed significant concern for a urine leak, delayed images were obtained. Increased tracer accumulation along the midline collection and low-level tracer uptake within the peritoneal cavity was seen 2 hours post-injection (Figure 3). This corresponded to the copious ascites

seen on CT (Figure 1). Interval reimplantation of the ureter into urinary bladder resulted in decreased volume of ascites and adequate generation of urine.

Conclusions/Discussion: Nuclear medicine renal scan can be used to diagnose a post-transplant intraperitoneal urinary leak. CT scans without IV contrast are often obtained after kidney transplantation, but they usually cannot be used to diagnose a leak due to low urine visibility. Technetium-99m MAG3 used in nuclear medicine renal scans concentrate in urine at doses not harmful to the kidneys. Typically, renal scintigraphy is obtained to assess for acute tubular necrosis or transplant rejection, and delayed images are not routinely obtained. However, the tracer uptake in the peritoneum seen in the delayed image in Figure 3 was the key to diagnosing the urine leak. The dynamic scan in Figure 2 was inconclusive for a leak: the observed midline collection could be misattributed to the bladder, despite a CT correlate. SPECT/CT may help for correlating the MAG3 signal to CT, but anatomic delineation in this case may still be challenging given the lack of IV contrast. Therefore, this case report demonstrates that delayed imaging on a nuclear medicine renal scan can offer precious insight when screening for a leak, helping with early diagnosis of post-transplant urological problems and thereby increasing the chances of successful treatment.

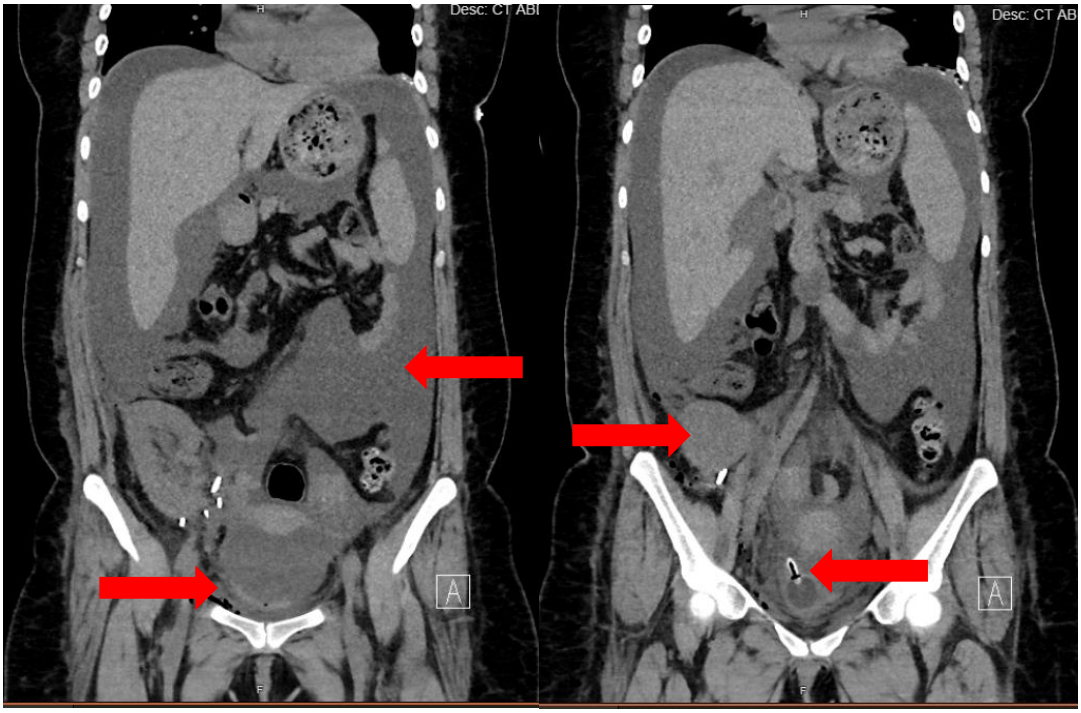

Figure 1. Coronal CT scans show ascites in the peritoneum, lack of hydronephrosis in transplant kidney, decompressed bladder, and urinary catheter.

Figure 2. Dynamic scans from renal scintigraphy shows radiotracer accumulation in newly transplanted kidney draining into a midline collection.

Figure 3. Delayed images from nuclear medicine renal scan show intraperitoneal urine leak.

References

1) Guimarães J, Araújo AM, Santos F, Nunes CS, Casal M. Living-donor and deceased-donor renal transplantation: Differences in early outcome–a single-center experience. Transplantation Proceedings [Internet]. 2015 May [cited 2023 Oct 24];47(4):958–62. Available from: https://www.sciencedirect.com/science/article/pii/S0041134515002365 doi:10.1016/j.transproceed.2015.03.008
2) Buttigieg J, Agius-Anastasi A, Sharma A, Halawa A. Early urological complications after kidney transplantation: An overview. World J Transplant. 2018 Sep 10;8(5):142-149. doi: 10.5500/wjt.v8.i5.142. PMID: 30211022; PMCID: PMC6134271.
3) Son H, Heiba S, Kostakoglu L, Machac J. Extraperitoneal urine leak after renal transplantation: the role of radionuclide imaging and the value of accompanying SPECT/CT - a case report. BMC Med Imaging. 2010 Oct 20;10:23. doi: 10.1186/1471-2342-10-23. PMID: 20961409; PMCID: PMC2984463.

Abstract for 36th Annual Northeast Regional Scientific Meeting (Revised)

Reassessment of Bone Loss in White Adult Females Ages 30 to 80 Years Old

Malcolm H. Blake*, John A. Vento and Fazle Hosain.

Division of Nuclear Medicine, Dept. of Diagnostic Imaging & Therapeutics, UCONN Health, Farmington, CT 06030.

Background: Measurements of bone mineral densities (BMD) of lumbar spines and proximal femurs with Dual-energy X-ray Absorptiometry (DXA) have been universally accepted for the assessment of osteoporosis. The peak bone mass attained in early life is a major determinant of fracture risk in later life. Now, a BMD measurement is recommended for all women >65 years regardless of additional risk factors.

Methods: The present study involves an analysis of bone mineral densities of 109 cases of normal white females, within the age range of 30 to 80 years, obtained early in 1990s by one of the authors (FH). They had no history of any fracture. They were neither on any exercise program, nor taking any medication for chronic illness. These were their first, and only, BMD measurements (g/cm2) with DXA as consenting volunteers. Here, we will focus on the lumbar spine (average of L2 to L4) and the femoral neck. Further, they were divided into 5 groups, successively at 10-year intervals of age. Each group was subjected to linear regressions: BMD versus Age. The slope (m) represented the rate of bone loss with respect to age within a decade. These values of 'm' were then plotted against the average age of women in each group in successive decades for regression analyses, especially for the quadratic equation. We also carried out similar analyses using some of the available reference data (e.g., Lunar Reference Data).

Results: Usually linear regression is performed (BMD vs Age) that provides a downward slope (m) representing the rate of bone loss. We got multiple 'm-values' corresponding to age range in successive decades. These values were not the same, suggesting a non-linear pattern of bone loss with advancing age. They correlated best with the average ages of corresponding groups for the quadratic function. It showed an accelerated rate of bone loss during the first few decades following menopause and thereafter it appeared to decelerate. The results obtained from similar analyses of other reference data confirmed our findings.

Conclusions: We, therefore, like to emphasize that medical assessment and intervention should be undertaken during the early years following menopause, rather than waiting until the individual attains age 65 as recommended. Early intervention is especially important for women with anticipated low peak bone mass. Any reduction in the rate of bone loss earlier in life will decrease the risk of bone fracture. Years ago, we undertook similar studies and observed possible acceleration in bone loss with advancing age, but we were not sure. The present reevaluation is relevant since it suggests modification in the clinical approach for treating post-menopausal women to reduce the risk of bone fracture.

*Present address: Desert Regional Medical Center, Palm Springs, CA 92262.

Incidental PSMA PET/CT Uptake in Hepatocellular Carcinoma and Liver and Splenic Hemangiomas

Deepak Kalbi[1], MD; Elliot Shulman[1], MD; Aspan Shokrekhuda[1], MD; Kwang Chun[1], Ana Valdivia[1], MD.

1 Department of Radiology, Division of Nuclear Medicine, Montefiore Medical Center/ The university Hospital for Albert Einstein College of Medicine

Background: PSMA PET/CT has emerged as a highly sensitive method for detecting prostatic cancer metastases. However, there have been reports of other pathologic lesions that express PMSA (prostate specific membrane antigen) and demonstrate increased uptake on PSMA PET/CT images. These pathologies include Malignant (such as gliomas, head and neck squamous cell carcinoma, thyroid cancer, breast cancer, thymoma, mesothelioma, hepatocellular carcinoma, cholangiosarcoma, adrenocortical carcinoma, hemangioma) and Benign (including thyroid and parathyroid adenomas, schwannoma, peripheral nerve sheath tumor, elastofibroma dorsi, pseudoangiomatous stromal hyperplasia of the breast, thymoma) cases. Additionally, inflammatory and infectious processes (such as thyroiditis neurocysticercosis, opacities and bronchiectasis, sarcoidosis, tuberculosis, anthracosilicosis) can also lead to elevated PSMA uptake on these images**Error! Hyperlink reference not valid.** [1][2].

Methods: We present four cases involving PSMA positive liver and splenic lesions which were not prostate cancer metastases, but instead represented sites of hepatocellular carcinoma (HCC) and hemangioma.

Results: In case one, a 67-year-old male exhibited increased PSMA uptake within a hepatic hemangioma. The second case involved a 79-year-old male with markedly increased PSMA uptake, which was confirmed as biopsy-proven HCC. In the third patient, an 82-year-old male, increased PSMA uptake was evident in a splenic hemangioma. Lastly, the fourth patient, a 58-year-old male with a history of prostate cancer, displayed significant increased PSMA uptake in the right hepatic lobe, potentially indicating a subcapsular mass, which subsequent MRI confirmed as HCC.

Conclusion: PSMA PET/CT is a recently developed and crucial imaging modality for evaluating prostate cancer metastases. As its use increases there are increasing reports of PSMA uptake in lesions other than prostate cancer. We have been able to identify four such cases involving lesions of the liver and spleen.

[1]de Galiza Barbosa F, Queiroz MA, Nunes RF, Costa LB, Zaniboni EC, Marin JFG, Cerri GG, Buchpiguel CA. Nonprostatic diseases on PSMA PET imaging: a spectrum of benign and malignant findings. Cancer Imaging. 2020 Mar 14;20(1):23. doi: 10.1186/s40644-020-00300-7. PMID: 32169115; PMCID: PMC7071711.

[2]Palot Manzil FF, Kaur H, Szabados L. Gallium-68 Prostate-Specific Membrane Antigen Positron Emission Tomography: A Practical Guide for Radiologists and Clinicians. Cureus. 2022 Mar 7;14(3):e22917. doi: 10.7759/cureus.22917. PMID: 35399427; PMCID: PMC8986511.

Title: Regaining lost market share following the SARS-COVID-19 (COVID) pandemic has proven difficult for lung scintigraphy.

Authors: Ara Mandjikian, Daniel Aharon, Abraham Kessler, Ghazaleh Mehdipoor, Mario Didea, Linda Haramati, Lionel Zuckier. Albert Einstein College of Medicine, Bronx, NY

Background: Onset of COVID initiated many changes in medical practice designed to provide appropriate care to patients while ensuring safety of healthcare workers. COVID virus infects the airways and may present like pulmonary embolism (PE). In addition, COVID has been associated with a hyper-coagulable state and thrombotic events, such as PE. Primary imaging methods of diagnosing PE are computerized tomography pulmonary angiography (CTPA) and pulmonary scintigraphy (VQ). Because of concern regarding aerosolization of virus, many COVID guidelines suggested avoiding ventilation studies, either performing perfusion studies alone as a screening exam, or shifting completely away from VQ to CTPA. The goal of this paper is to track utilization of PE studies in our large healthcare network, where VQ use has been historically high, during the SARS-COVID-19 pandemic and its aftermath.

Methods: Using PowerM (Montage), we conducted a retrospective study within our large urban hospital center to identify patients studied for evaluation of PE by VQ or CTPA from Sept 2019 to Sept 2023 (n=38,550). Frequency of COVID-related hospital admissions in Bronx County was obtained from public sources. Ventilation-only and full VQ studies were differentiated by review of technique in each report. Data were binned on a per-month basis. Results were correlated with the period when ventilation scans were omitted. Statistical significance was determined at the 0.05 level using Student's unpaired t-test.

Results: VQ utilization decreased from 204±17 (mean±SD) scans per month over the 6 month period prior to March 2020 (outbreak month) to a monthly average rate of 52±27 scans during April to Sept 2020 (75% decrease, $p<.0001$). Concurrently, monthly CTPA utilization decreased from 582±35 during the 6 months before March to an average of 552±66 cases during 6 months following March (9% decrease, $p=.1739$, NS). During the subsequent 31 months (Oct 2020 through April 2023) prior to the formal end of the pandemic (May 11, 2023), VQ use averaged 77±14 per month (62% decrease compared to baseline) while CTPA averaged 725±89 per month (25% increase compared to baseline). In the 4 months following the pandemic's end, monthly utilization was 79±10 (39% baseline) and 893±26 (153% baseline), respectively. Small trends in utilization appear to correspond to initial COVID waves. Scintigraphy constituted 25.9% of total pre-COVID baseline PE studies (CTPA and VQ) performed between Sept 2019 and Feb 2020, decreased to a nadir of 6.7% in the 6 months following outbreak of the pandemic, and has stabilized at only 8.1% of total PE studies in the 4 months since official end of the pandemic.

Conclusions: Utilization of VQ for the diagnosis of PE acutely decreased following arrival of the pandemic and continues to remain at approximately 1/3 of prepandemic levels, while CTPA has increased by more than 50% compared to baseline. Even after return to original protocols and an official end to the pandemic, utilization of scintigraphy remains markedly decreased from pre-pandemic levels.

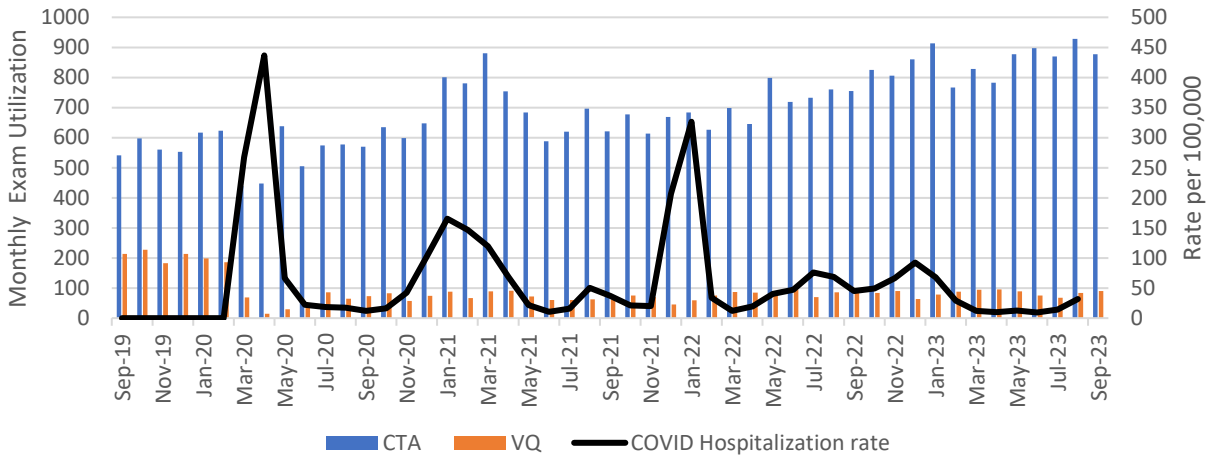
Monthly Exam Utilization
1000
900
800
700
600
500
400
300
200
100
0
Rate per 100,000
500
450
400
350
300
250
200
150
100
50
0
Sep-19
Nov-19
Jan-20
Mar-20
May-20
Jul-20
Sep-20
Nov-20
Jan-21
Mar-21
May-21
Jul-21
Sep-21
Nov-21
Jan-22
Mar-22
May-22
Jul-22
Sep-22
Nov-22
Jan-23
Mar-23
May-23
Jul-23
Sep-23
CTA
VQ
COVID Hospitalization rate

A Pictorial Review of Visceral Sites of Metastatic Prostate Cancer in PSMA PET/CT

Authors: Gabriela Cepeda De Jesus, MD, Jonathan Nazha, MD, Steven Robinson, DO, Prasanta Karak, MD.

Department of Radiology, Hartford Hospital, Hartford, CT

Background: Prostate cancer (PC) is the second most common malignancy in men worldwide. In 2023, it is estimated that there will be 288,300 new cases of prostate cancer and 34,700 disease-related deaths in the United States.

The PC staging system uses anatomic (TNM) information, pre-treatment serum PSA level, and histologic grade group to define prognostic stage groups. The TNM classification for PC subdivides metastatic disease into M1a (nonregional lymph nodes), M1b (bones), and M1C (other site(s) with or without bone disease).

Prostate-specific membrane antigen (PSMA) PET/CT is a relatively new imaging modality that has revolutionized PC staging. Current NCCN guidelines recommend PSMA PET/CT as the preferred bone and soft tissue imaging modality in intermediate and high-risk patients. The purpose of this study is to describe the frequency and sites of visceral PC metastases on PSMA PET/CT.

Method: All available 535 PSMA PET/CT studies performed at our institution between September 2021 and September 2023 were retrospectively reviewed, from which 65.6% (351/535) were done for biochemical recurrence and 34.4% (184/535) were done for initial staging. Visceral metastatic sites were identified in 29 out of 535 (5.4%) PSMA PET/CT, from which 26 out of 29 (89.7%) were performed for biochemical recurrence and 3 out of 29 (10.3%) for initial staging. Histopathological confirmation was obtained in five cases.

Results: The most frequent sites of visceral metastases identified on PSMA PET/CT were the lungs (59%, 17/29), liver (21%, 6/29), and adrenal glands (17%, 5/29). There was one case of local recurrence in the rectum and another with a metastatic soft tissue nodule in the subcutaneous fat of the upper back. We present a pictorial review of some of these metastatic PC cases.

Conclusion: PSMA PET/CT allows for the detection of visceral sites of prostate cancer metastasis, with common sites being the lungs, liver, and adrenal glands. In our study, visceral metastasis was detected in 5.4% of all the patients who underwent PSMA PET/CT. The timely detection of these lesions allows proper anatomical staging, which will determine subsequent management and prognosis.

Figure 1. A 79-year-old man with prostate cancer (Gleason 3+4) diagnosed in 2011 status post prostatectomy. Serum PSA at the time of PET/CT: 2.89 ng/mL. F18-PSMA PET/CT: Axial PET and sagittal PET/CT fused images demonstrate focal uptake in the rectal wall. Axial CT image demonstrates corresponding asymmetric rectal wall thickening. An endoscopic biopsy was performed confirming recurrent prostatic adenocarcinoma.

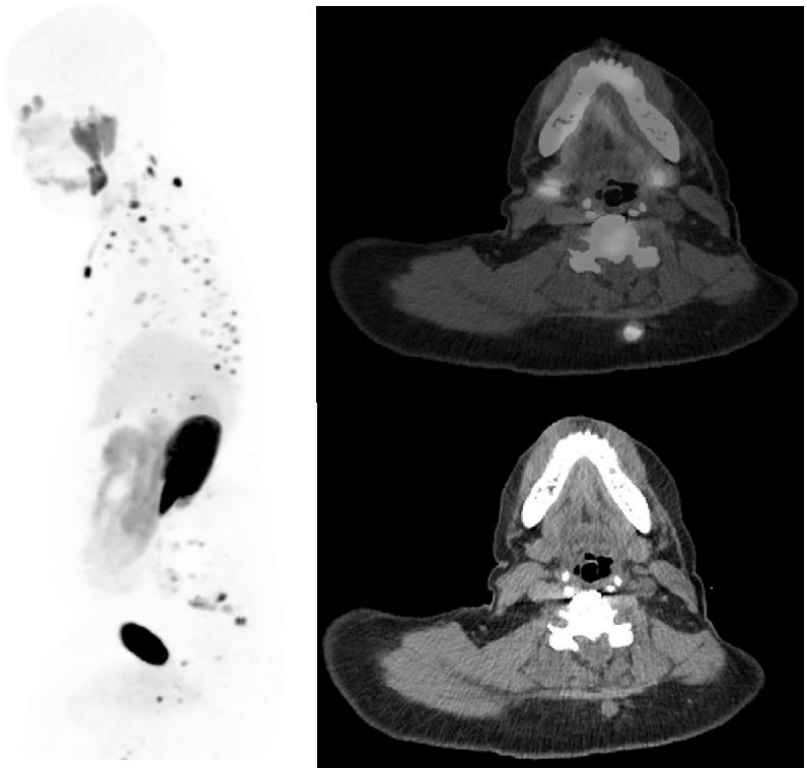

Figure 2. A 58-year-old man with metastatic castrate-resistant prostate cancer diagnosed in 2018 on docetaxel and androgen deprivation therapy. Serum PSA at the time of PET/CT: 79.87 ng/mL. Ga68-PSMA PET/CT: Sagittal MIP images demonstrate extensive uptake throughout the axial skeleton, most consistent with osseous metastases. Axial CT and PET/CT fused images demonstrate focal uptake in a soft tissue nodule posterior to the C6 vertebral body within the subcutaneous fat. A CT-guided biopsy confirmed metastatic prostatic adenocarcinoma at this site.

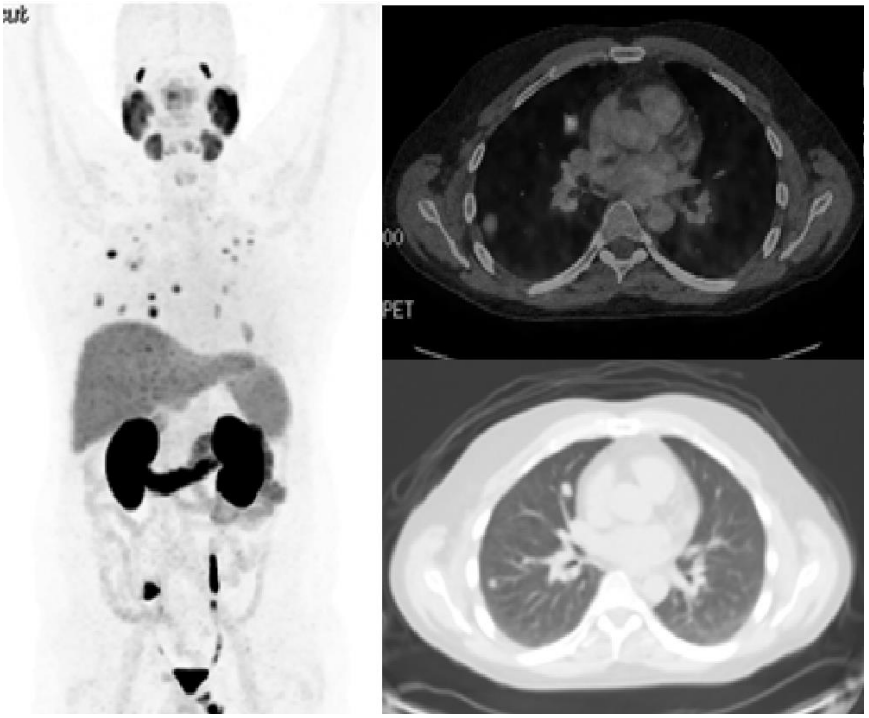

Figure 3. 48-year-old man with prostate cancer (Gleason 5 + 4) diagnosed in 2019, treated with ADT and pelvic radiation. Serum PSA at the time of PET/CT: <0.02 ng/mL. Ga68-PSMA PET/CT (2022): MIP image shows multifocal uptake in both lungs and mediastinum. A PSMA-avid lesion in the right sacrum is also noted. Axial CT and PET/CT fused images demonstrate focal uptake in the pulmonary nodules, histologically-proven metastatic prostatic adenocarcinoma.

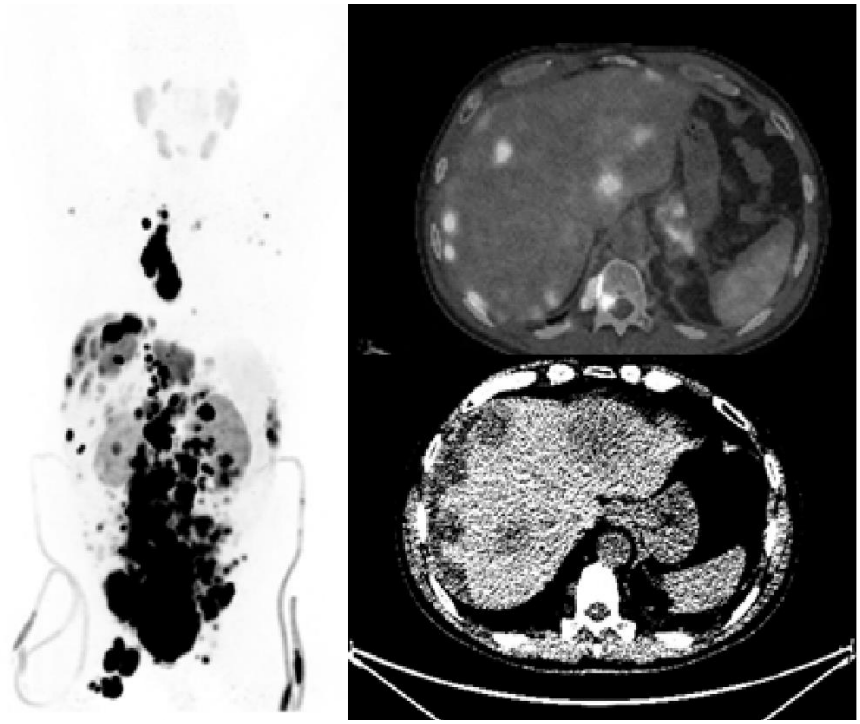

Figure 4. 60-year-old male with metastatic prostate cancer at initial diagnosis in 2020, treated with ADT and docetaxel. PSMA PET/CT was performed as pre-evaluation for Pluvicto therapy in 2023. Serum PSA 3 months prior to PET/CT was 185.00 ng/mL. Ga68-PSMA PET/CT: MIP image shows extensive locoregional and distant PSMA-avid disease involving inguinal, abdominopelvic, mediastinal and axillary lymph nodes. Axial CT and PET/CT fused images demonstrate multiple PSMA-avid liver metastases.

The Increasing Value of ^{18}F-FES PET Imaging in the Clinic

Mehdi Djekidel, MD, Joshua Lim, MD, Josephine N. Rini, MD

Background:

Breast cancer is the most common cancer in the United States and the fourth most lethal cancer in women. Survival rates have improved over the past twenty years owing to earlier diagnosis and improved therapeutics. Imaging has traditionally played a crucial role in screening, early diagnosis, initial staging, restaging and response to treatment assessment. This includes the use of morphological imaging techniques, such as mammography, ultrasound, MRI and CT, and functional imaging techniques, such as FDG-PET. Recently, with the approval of ^{18}F-fluoroestradiol (FES)-PET for the detection of estrogen receptor (ER) positive lesions, a new paradigm is emerging. This technique is gaining traction a problem-solving tool in breast cancer management in several clinical scenarios. It also is showing promise in becoming a standard of care tool in the evaluation of patients with invasive lobular breast cancer. Proper and wider use of this technique requires increased awareness and knowledge on the part of nuclear medicine experts, as well as referring physicians. Additionally, precision medicine tools offering a comprehensive noninvasive whole-body evaluation of specific molecular phenotypes are needed to accomplish a personalized medicine paradigm. Considering heterogeneity of disease is an important factor in various cancers, including breast cancer, and FES-PET can aid in the management of these patients.

Methods:

We illustrate 3 cases where FES-PET served as an important problem-solving technique. We review the FES Appropriate Use Criteria (AUC) and share a roadmap for clinical use.

Results:

Case 1: Recurrent ER-positive brain metastasis

A 56 y.o. F with a h/o breast Ca metastatic to brain s/p SBRT, underwent FES-PET/CT due to brain MRI concerning for tumor recurrence. FES-PET fused with separately acquired MRI showed increased avidity throughout the lesion, compatible with recurrent ER-positive brain metastasis.

Case 2: Newly diagnosed ER-positive breast Ca and lymphoma

A 66 y.o. F with newly diagnosed ER-positive left breast cancer had a preoperative FDG-PET/CT which showed multiple FDG-avid lymph nodes above and below the diaphragm and an indeterminate FDG-avid rib lesion. Percutaneous needle biopsy of left axillary node was positive for follicular lymphoma. She underwent left breast lumpectomy and left axillary sentinel node biopsy. Pathology was positive for invasive lobular carcinoma. One axillary lymph node was positive for metastasis, and a second node was positive for follicular lymphoma. Postoperative FES-PET showed no evidence of ER-positive disease. FDG-avid lymphadenopathy was presumed to be secondary to lymphoma and rib lesion was favored to be benign.

Case 3: Recurrent metastatic lobular breast cancer

An 89 y.o. F with a remote h/o ER-positive lobular breast Ca was found to have an expansile rib lesion on CT. A bone scan showed a solitary, indeterminate rib focus, corresponding to lesion seen on CT. FES-PET/CT showed multiple FES-avid osseous metastases in the axial skeleton and left femur, with corresponding lytic lesions, or no corresponding abnormalities on CT. A subsequent biopsy of the rib lesion confirmed metastatic breast Ca.

Conclusion:

FES-PET is a potentially valuable tool in the management of breast cancer patients. Increased awareness and knowledge are essential to improve patient access to FES-PET.

Increasing Utilization of FDG-PET/CT for Imaging Infection/Inflammation

Joseph E. Glaser, MD, Christopher G. Caravella, MHA, LNMT, Josephine N. Rini, MD

Background:

FDG-PET/CT detects areas of increased glucose utilization which occur in malignancy and infectious/inflammatory conditions. While predominantly used for oncologic imaging, FDG-PET/CT also has shown utility for imaging infectious/inflammatory conditions, including fever of unknown origin, osteomyelitis, and cardiovascular conditions, such as cardiac sarcoidosis, infective endocarditis, infection of implantable cardiac devices and vasculitis. In 2017, we introduced an FDG-PET/CT protocol for imaging cardiac sarcoidosis, but until recently the use of FDG-PET/CT for other infectious/inflammatory conditions was limited due to lack of reimbursement. In January 2021, Centers for Medicare and Medicaid Services (CMS) retired the National Coverage Determination (NCD) for the non-coverage of FDG-PET for infection/inflammation, delegating coverage for these indications to the local Medicare Administrative Contractors (MACs). Following this decision, we implemented operational changes to streamline ordering, billing, scheduling, and image acquisition for infectious/inflammatory conditions. We describe these operational changes, summarize our experience with FDG-PET/CT for infectious/inflammatory indications, and illustrate case examples.

Methods:

Following the January 2021 decision by CMS, we implemented the following operational changes: 1. Created infection/inflammation-specific FDG-PET/CT electronic medical record (EMR) orderables tied to non-oncologic unified item masters (UIMs) (Figure 1). 2. Developed Ask at

Order Entry (AOE) questions to reduce ordering errors and to guide the referring service to the appropriate imaging protocol (Figure 2). 3. Designed Radiology Information System (RIS) procedures and scheduling activities for infection/inflammation to distinguish these indications from oncologic PET (excluded initial staging/restaging modifiers required for oncologic PET billing). 4. Established pre-scheduling workflows to facilitate physician review of infection/inflammation referrals, prior-authorization verification, and accurate scheduling. 5. Expanded cardiac sarcoidosis FDG-PET preparation to include all infections of the myocardium and infection of implantable cardiac devices, to suppress physiologic uptake of FDG. We subsequently searched the radiology reporting system to determine annual PET/CT volumes for cardiac sarcoidosis and all other infectious/inflammatory indications from January 2017 through September 2023. We selected three cases from our institution to illustrate the utility of FDG-PET/CT for imaging infectious/inflammatory conditions.

Results:

Utilization of FDG-PET/CT for cardiac sarcoidosis has increased since 2017, and utilization of FDG-PET/CT for other infectious/inflammatory conditions has increased since 2022, as shown in Figure 3. While most commercial payers follow CMS coverage guidance, some continue to deny PET for infection/inflammation. Case examples from our institution showing FDG-PET/CT for cardiac sarcoidosis, fever of unknown origin, and infection of an implantable cardiac device are shown.

Conclusion: We have seen increased utilization of FDG-PET/CT for imaging cardiac sarcoidosis and other infectious/inflammatory conditions in clinical practice. The CMS decision to retire the NCD for the non-coverage of FDG-PET for infection/inflammation in 2021, and the operational changes that were subsequently implemented, have facilitated this trend. We anticipate that the utilization of FDG-PET/CT for infectious/inflammatory indications will continue to increase and that coverage by private payers will expand.

Prostate Cancer Whole-Body Bone Scan Utilization after Introduction of PSMA PET/CT

Jermaine Osei-Tutu, Paige Bennett, Christopher Caravella, Josephine Rini, Christopher J. Palestro, Kenneth J. Nichols
Donald and Barbara Zucker School of Medicine at Hofstra/Northwell, Hempstead NY; USA

Background: Introduction of new radiopharmaceuticals can cause changes in clinical practice patterns that substantially affect workflow in nuclear medicine clinics. We observed at our university-based imaging centers that when prostate specific membrane antigen (PSMA) PET/CT became available for staging & restaging prostate cancer, the volume of bone scans performed on pts with prostate cancer (BS-P) markedly decreased. We aimed to study utilization patterns of PSMA PET/CT & BS-P during the four-year period around US FDA approval of PSMA PET/CT in December 2020 & implementation of PSMA PET/CT at our imaging centers. We tested the hypothesis that the decline of BS-P accelerated following US FDA approval, as physicians planned for use of PSMA PET/CT for initial staging & restaging in their pts.
Methods: For this clinical utilization analysis project, our imaging centers' clinical report system was searched for BS-P & PSMA PET/CT from January 2019 through June 2023. Clinical implementation at our centers occurred in Quarter 3 of 2021. Bone scans were performed using standard protocols & included whole body imaging & SPECT/CT as needed. PSMA PET/CTs were performed using standard protocols & included imaging from the skull vertex to the knees. Quantitative & statistical analysis was performed.
Results: Annualized average monthly BS-P cases peaked at 53.7 cases/month in 2021, then subsequently decreased progressively over time. There were 552 BS-P performed in 2019, 503 in 2020, 614 in 2021, 481 in 2022 & 152 in the first half of 2023. There were 30 PSMA PET/CT scans in 2021, 455 in 2022 & 384 in the first half of 2023. BS-P monthly averages declined by 22% from 2021 to 2022 & by 36% from 2022 to 2023, while PSMA PET/CT monthly averages increased by 1,416% from 2021 to 2022 & by 69% from 2022 to 2023. These dramatic changes occurred after US FDA approval of PSMA PET/CT in mid-2021. There was a significantly greater decline in BS-P cases from 2022 to 2023 compared to 2021 to 2022 (36% vs 22%, $p < .0001$). The steepest quarterly decline in BS-P cases (43%) in 2020 Q2 coincided with the COVID pandemic, while the greatest quarterly increase in PSMA PET/CTs (400%) occurred at the outset of PSMA PET/CT implementation in Q4 of 2021. The decline in BS-P as PSMA PET/CT utilization increased continued into Q2 2023, when the percentages of PSMA PET/CT & BS-P were 74% & 26% ($p < 0.0001$) out of total cases, respectively.
Conclusions: At our imaging centers, the utilization of bone scans for prostate cancer has declined & correlates with timing of US FDA approval & implementation of PSMA PET/CT for initial staging & restaging of pts with prostate cancer, thus illustrating workflow changes when new agents are introduced that affect clinical management options.

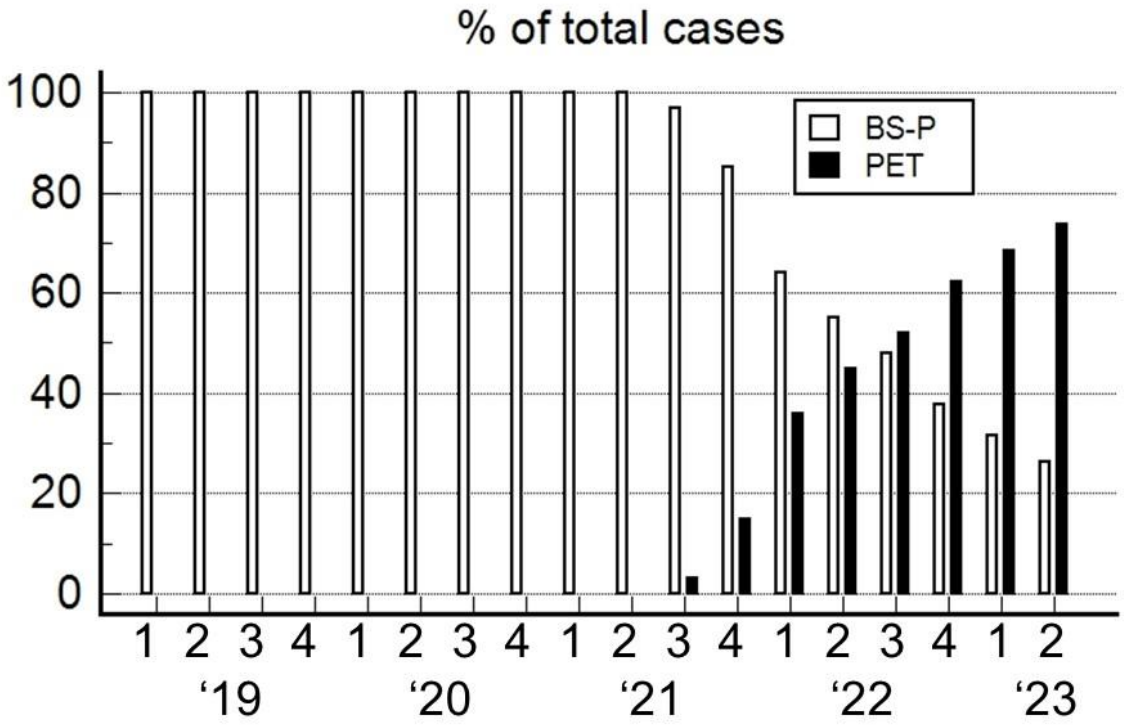
% of total cases
100
80
60
40
20
0
BS-P
PET
1 2 3 4 1 2 3 4 1 2 3 4 1 2 3 4 1 2
‘19
‘20
‘21
‘22
‘23

Title: A Case of Incidental Anaplastic Thyroid Carcinoma Detected on ^{18}F-PSMA PET/CT

Authors: Veronica Pereira, MD, Gabriela Cepeda, MD, Prasanta Karak, MD
Affiliation: Department of Radiology, Hartford Hospital, Hartford, CT

Background:
Anaplastic thyroid carcinoma (ATC) is a rare and highly aggressive form of thyroid carcinoma accounting for approximately 2-3% of all thyroid neoplasms[1]. ATC carries a poor prognosis secondary to multiple factors including extensive local invasion and distant metastatic spread at presentation, as well as poor response to usual treatments used in differentiated thyroid cancers such as thyroid stimulating hormone suppression and radioactive iodine (RAI) therapy[1].

Prostate-specific membrane antigen (PSMA) is a transmembrane glycoprotein receptor that is expressed in normal prostatic tissue and considerably more so in prostate carcinoma, making it a useful target for imaging and therapy for prostate cancer[2]. However, wide use of PSMA PET/CT for prostate imaging has resulted in unexpected detection of non-prostatic tumors including carcinomas of the lung, breast, colorectum and thyroid neoplasms. While previous studies have described PSMA expression on PET/CT in well-differentiated thyroid cancers, few studies have examined PSMA expression in ATC.

Methods: This case report describes the incidental detection of ATC in a patient undergoing ^{18}F-PSMA PET/CT for long-standing history of prostate cancer.

Case Description/Results:
82-year-old African American male with a remote history of colon cancer treated with surgical resection and adjuvant chemotherapy as well as a long-standing history of grade group 1 prostate cancer diagnosed 10 years prior and managed with active surveillance was referred for ^{18}F-PSMA PET/CT secondary to a rising PSA level, 115.4 ng/mL at time of referral, and concern for metastatic disease.

^{18}F-PSMA PET/CT was performed and demonstrated prostamegaly with avid PSMA uptake (SUVmax= 12.7). No metastatic lesion for prostate cancer was identified. However, there was an intensely PSMA-avid 7 cm mass arising from the right thyroid lobe with substernal extension (SUVmax= 17.5). Thyroid ultrasound and fine-needle aspiration biopsy were performed, with initial pathology consistent with papillary thyroid carcinoma (PTC).

Subsequently, the patient underwent thyroidectomy with level VI lymph node dissection. Final pathology demonstrated anaplastic thyroid carcinoma with positive margins and lymphovascular invasion, arising in association with PTC. One month following surgery, approximately 5 months from the previous PSMA scan, ^{18}F-FDG PET/CT demonstrated recurrent/residual FDG-avid lesion in the right thyroidectomy bed extending into the upper mediastinum (SUVmax= 53.2), and FDG-avid bilateral lung metastases (SUVmax= 36.7), findings consistent with stage IV metastatic disease. Of note, multiple small bilateral pulmonary nodules under 0.5 cm were seen on the initial PSMA PET/CT but were too small to characterize.

Over the course of one year, the patient has undergone 20 cycles of immunotherapy with pembrolizumab with continued positive treatment response and no evidence of disease progression.

Conclusions:

PSMA expression has previously been described in well-differentiated thyroid cancers, however, few studies have examined PSMA expression in anaplastic thyroid cancer. This case describes an incidental thyroid lesion discovered on ^{18}F-PSMA PET/CT imaging, ultimately found to be anaplastic thyroid cancer arising in association with papillary thyroid cancer. Further studies aimed at understanding patterns of PSMA expression on PET/CT in these poorly differentiated tumors might provide further grounds for evaluation of PSMA-targeted radioligand therapy, especially given the relative lack of therapeutic options in anaplastic thyroid cancer.

References:

1. Faten Limaiem, Anis Rehman, & Mazzoni, T. (2019, October 2). *Cancer, Papillary Thyroid Carcinoma (PTC)*. Nih.gov; StatPearls Publishing. https://www.ncbi.nlm.nih.gov/books/NBK536943/
2. Bychkov, A., Vutrapongwatana, U., Tepmongkol, S., & Keelawat, S. (2017). PSMA expression by microvasculature of thyroid tumors – Potential implications for PSMA theranostics. *Scientific Reports*, *7*(1). https://doi.org/10.1038/s41598-017-05481-z

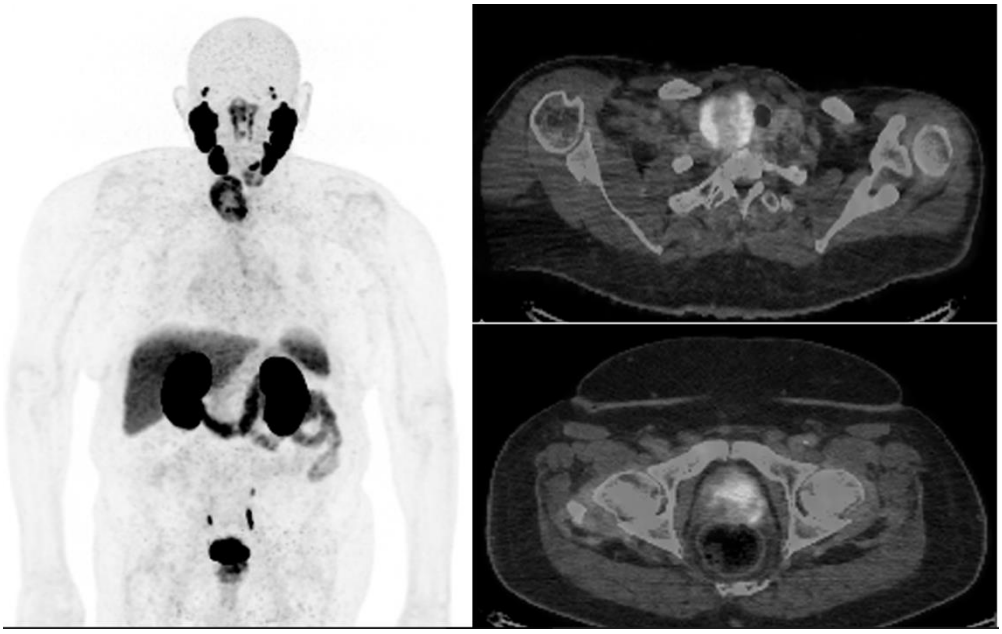

Figure 1. ^{18}F-PSMA PET/CT: Axial PET/CT fused *(top right*) and MIP images show heterogenous PSMA uptake in a large right thyroid lobe nodule, subsequently pathology-proven ATC. Axial PET/CT fused image *(bottom right)* shows heterogenous PSMA uptake in the prostate gland, consistent with known prostate cancer.

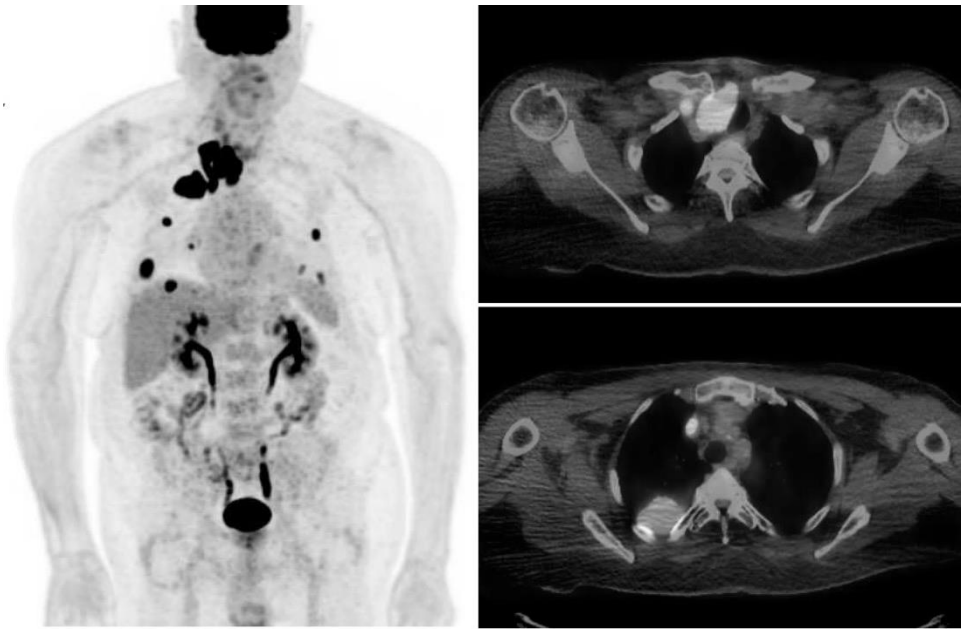

Figure 2. ^{18}F-FDG PET/CT: Axial PET/CT fused image (*top right*) shows intense FDG-avid lesion in the right thyroidectomy bed. A small focus of FDG uptake lateral to this lesion corresponds to tumor thrombus in the superior vena cava/right internal jugular vein. MIP and axial PET/CT fused images (*bottom right*) show multiple FDG-avid lung metastases.

Utility of Somatostatin Receptor PET Imaging in Benign and Inflammatory Disorders

William Y. Raynor, MD[1], Stephen J. Sozio, DO[1], Jeffrey S. Kempf, MD[1]

1. Department of Radiology, Rutgers Robert Wood Johnson Medical School, New Brunswick, NJ, USA.

Background: A peptide hormone which exerts its effects by binding to G protein-coupled receptors, somatostatin is mostly known for its role in regulating nervous and gastrointestinal systems. Tissues which express high density of somatostatin receptors (SSTR) are found in the spleen, liver, pancreas, thyroid gland, and adrenal glands. In addition, activated lymphocytes and macrophages express high levels of SSTR. Positron emission tomography (PET) imaging using SSTR agonists (namely, DOTATATE, DOTATOC, and DOTANOC) labeled with ^{68}Ga and ^{64}Cu can detect neuroendocrine tumors (NETs), which often express high levels of the SSTR2 subtype. The introduction of ^{177}Lu-labeled DOTATATE represented a breakthrough in nuclear medicine theranostics, becoming the first FDA-approved radiopharmaceutical for peptide receptor radionuclide therapy. Besides NETs, meningiomas have also been successfully imaged with SSTR PET, with proposed uses in diagnosis, treatment planning, and evaluation for recurrence. As SSTR PET continues to gain increased use for these established indications, preliminary investigations have reported new applications for this technology, particularly in the assessment of inflammation. We aim to review and discuss the evidence regarding the use of SSTR PET in assessing benign, non-neoplastic disorders.

Methods: A literature review was conducted using PubMed with "DOTATATE," "DOTATOC," and "DOTANOC" as keywords. Results pertaining to neoplasms such as NETs, pheochromocytomas, paragangliomas, and meningiomas were excluded. Original articles and case reports pertaining to benign applications of SSTR PET were then used to create a comprehensive review.

Results: High sensitivity and specificity have been reported for ^{68}Ga-DOTANOC PET/CT in the diagnosis of systemic sarcoidosis, with a corresponding decrease in tracer avidity following response to therapy. The performances of both ^{68}Ga-DOTANOC and ^{68}Ga-DOTATATE in assessing cardiac sarcoidosis have been compared to that of ^{18}F-fluorodeoxyglucose (FDG), with conflicting results between studies. Several studies have also used SSTR radiotracers to evaluate atherosclerosis in the aorta, carotid arteries, and coronary arteries, which not only showed that this method is feasible, but also that response to therapy is readily apparent using SSTR PET. A variety of additional benign disorders amenable to imaging with SSTR PET have been described with only case reports or small preliminary studies for support. Specifically, a case report and a single prospective study have suggested the ability to assess large vessel vasculitis using ^{68}Ga-DOTATATE PET/MRI. Early investigations suggested the feasibility of imaging tuberculosis, endometriosis, and pulmonary fibrosis with SSTR PET. Case reports have also suggested potential roles for SSTR PET in Graves ophthalmopathy and IgG4-related disease.

Conclusions: In this review, we report the emerging use of SSTR PET in benign and inflammatory conditions. Preliminary data suggest there may be a potential role for SSTR PET to diagnose and guide therapy for atherosclerosis and systemic sarcoidosis. Additional

applications such as imaging of large vessel vasculitis and pulmonary fibrosis may be possible, although further investigations are warranted.

Managing 90Y waste in an effort to increase space in the Nalgene bottle and reduce possible contamination.

Lena Samad[1], Eugenio Silvestrini[2,3]

1 Hofstra University, Hempstead, NY

2 Department of Radiology, Radiation Safety, Northwell Health, Manhasset, NY

3 Department of Physics and Astronomy, Hofstra University, Hempstead, NY

Background

90Y glass microsphere Therasphere therapy is a form of internal radiation therapy aimed at hepatocellular carcinoma. 90Y, a strong beta emitter, is deposited in the tumor via the hepatic artery. Each sphere is approximately 20-30 μm in diameter. Due to the vasculature of the liver, the spheres are generally engulfed by the tumor and begin the radiation therapy process. The betas have a short penetration range of approximately 2.5 mm in tissue, causing limited damage to the rest of the normal liver. In addition to the vial containing the dose is the sterile ‘“Therasphere Administration kit” containing a top shield, acrylic box base, electronic radiation dosimeter and a normal saline solution bag hook. The spheres are settled in a 0.3 mL “vee-bottom” vial containing pyrogen-free water fluid shielded in a lead container. While the set-up procedure is quite simple, the waste disposal can get tricky to handle. Therasphere waste must be disposed of properly, and it is recommended that a 2 L “wide-mouth waste” polyethylene jar be used. Once the spheres are transferred to the treatment site, the empty vial, the clamps, the catheter used, the surgical towels, the connection port, and any other supplies utilized during the procedure that may be contaminated, are transferred into this 2 L jar. The jar overflows quickly with minimal room to even close the lid on the container. In an effort to control waste

management and lower the probability of a spill or contamination from the spheres, this project is aimed to remove the waste that is not radioactive and dispose of it separately. This will provide more space for the Physicians performing the procedure to properly and effortlessly dispose of the contaminated waste swiftly and with ease, while also potentially placing the “hot spot” in front of the sensitive volume of the ion chamber for post treatment jar survey.

Methods

The purple cap sealing the vial, the alcohol swab used to disinfect the septum, and the plug that covers the septum were tested. Both solid and liquid scintillators were used and the counts per minute were recorded and compared to the background.

Results

The resulting counts were shown to be indistinguishable from background. The purple seal has the closest value to the background. The plug was tested next in the solid scintillator, and then completely covered in econo-safe solution prior to being placed in a liquid scintillator. Lastly, the alcohol pad is the closest material to the source, and since the alcohol pad also came back with negligible counts, it is safe to say that overall, there is little-to-no contamination of these components of the set.

Conclusion

As such, the purple seal, the vial plug and the alcohol swab used to clean the top of the vial can be disposed of in nonradioactive waste, thereby reducing the overall amount of post-procedural radioactive waste.

The utility of Trabecular Bone Score (TBS) in the evaluation of lung transplant candidates

Alain E. Sherman, MD, MBA, Aspan M. Shokrekhuda, MD, Deepak P. Kalbi, MD, & Kwang J. Chun, MD

Montefiore Medical Center/Albert Einstein College of Medicine

Abstract

Background: Lung transplant candidates routinely undergo bone mineral density (BMD) screening using dual-energy X-ray absorptiometry (DXA) due to increased risk of osteoporosis and related fractures secondary to comorbidities and prolonged immunosuppression. Nonetheless, postoperative fractures have been well-documented, even in patients with normal BMD. Trabecular Bone Score (TBS) has emerged as a complementary index of bone microarchitecture and independent predictor of fracture risk that has been seldom studied in this population. The present study sought to investigate the value of TBS, in conjunction with DXA, for the evaluation of osteoporosis in lung transplant candidates.

Methods: A retrospective review of 191 DXA scans of patients undergoing lung transplantation at a large, urban, academic medical center was performed. The mean age of the sample was 62.0 (SD = 9.7), with a modest male predominance (61.8%) and relatively diverse racial/ethnic composition (46.3% Hispanic, 29.4% white, 21.9% black). TBS was calculated using DXA images of the lumbar spine. Patients were classified by BMD and microarchitectural integrity using established T-score cutoffs for DXA and TBS, respectively.

Results: Differences in the observed rates of osteopenia (36.6%), osteoporosis (11.0%), partially degraded bone (38.7%), and degraded bone (33.5%) were statistically significant, $p < 0.001$. Significantly more patients were found to have abnormal bone according to TBS (72.3%) compared to DXA (47.6%), $p < 0.001$. Whereas TBS and DXA T-scores were moderately correlated, $r = 0.50$, $p < 0.001$; TBS T-scores ($M = -1.97$, SD = 1.31) were, on average, significantly lower than DXA T-scores ($M = -0.79$, SD = 1.56), $t(190) = 11.17$, $p < 0.001$. There were 153 cases (80.1%) for which the TBS T-score was less than the corresponding DXA T-score. There was no statistically significant difference in mean DXA T-scores between male (*M*

= -0.67, SD = 1.50) and female patients (M = -0.99, SD = 1.65), $t(189) = 1.40$, $p = 0.16$. However, women (M = -2.40, SD = 1.50) had significantly lower mean TBS T-scores than men (M = -1.71, SD = 1.10), $t(189) = 3.58$, $p < 0.001$. Hispanic patients (M = -1.13, SD = 1.56) had significantly lower BMD compared to white (M = -0.40, SD = 1.13) or black patients (M = -0.12, SD = 1.68), $F(4, 155) = 5.67$, $p < 0.001$. In contrast, microarchitecture did not differ by race/ethnicity, $F(4, 155) = 0.35$, $p = 0.84$.

Conclusions: Like osteoporosis, impaired trabecular microarchitecture is extremely common among lung transplant candidates. A substantial proportion of patients remain at risk of fracture through degraded bone despite normal BMD. TBS offers promise as a simple, inexpensive, noninvasive, and readily available adjunct to DXA in this unique and vulnerable population. Interestingly, TBS may be robust against racial/ethnic disparities traditionally encountered in BMD screening.

Table 1. Bone health profiles of lung transplant candidates according to DXA and TBS

T-Score	DXA		TBS	
$T \geq -1$	Normal	100 (52.4%)	Normal	53 (27.7%)
$-2.5 < T < -1$	Osteopenia	70 (36.6%)	Partially Degraded	74 (38.7%)
$T \leq -2.5$	Osteoporosis	21 (11.0%)	Degraded	64 (33.5%)

Abstract

Carcinoid Crisis in Lutetium-177-Dotatate Therapy: A Review

Stephen Sozio, DO, MBS[1], William Raynor, MD[1], Marc Chaise, MD[1], Lenore Giangrasso, CNMT[2], Anthony Yudd, MD, PhD[1], Jeffrey Kempf, MD, FACR[1]

1. Rutgers Robert Wood Johnson Medical School, New Brunswick, NJ
2. Robert Wood Johnson University Hospital, New Brunswick, NJ

Background: Neuroendocrine tumors (NET) are a diverse group of malignancies which account for an average of less than 1% of all malignancies diagnosed in the United States each year [1]. Neuroendocrine tumors typically express somatostatin receptors on their cell surface, which exert inhibitory effects on growth when bound to somatostatin. Management typically first involves initiation of a somatostatin analog (such as octreotide) to control symptomatology and tumor growth, and a subsequent combination of surgical resection, organ-targeted chemoembolization, and/or radionuclide therapy [1].

Lutetium-177-Dotatate (Lutathera®), a combined radionuclide-peptide, selectively binds to and is internalized by cells expressing somatostatin receptor, where beta-emission results in free radical generation and subsequent cell destruction [2]. While multiple studies have demonstrated efficacy of this radionuclide in the treatment of NETs, this therapy is not without risk, with the most common adverse effects being nausea/vomiting, transaminitis, anemia, and electrolyte imbalance, and with rarer complications including renal impairment and myelodysplastic syndrome [2]. Of importance, carcinoid crisis (CC) is a rare but potentially life-threatening complication of therapy, causing a range of symptoms including hemodynamic instability, arrythmia, and potentially death [3]. Given the comparative rare incidence of CC, this abstract provides a comprehensive literature review of the topic to promote awareness of the pathology with emphasis on early recognition and management.

Methods: A comprehensive literature review of lutetium-177-dotatate therapy with attention to reports concerning carcinoid crisis was performed. We reviewed reported incidence, presentation, symptomatic management, and preventative measures. Additionally, we provide review of our own institution data to provide our own institution's incidence of CC.

Results: The most common symptoms of CC include flushing, diarrhea, tachycardia, and altered mental status, and are most commonly encountered within 12-48 hours of receiving the first dose [3,4]. While several case reports have documented patients requiring hospital admission for management of CC under this circumstance, no documented deaths directly attributed to

lutetium-177-dotatate-associated CC have been recorded [5]. The incidence of CC is ranges between 1-2% of treatment recipients, although the exact incidence is not well known, in part due to poor definition of criterion qualifying diagnosis of the pathology [4]. Patients with tumors located within the small intestine or right-sided colon, higher tumor burden, metastatic disease to the liver, and high levels of 5-hydroxyindolacetic acid and chromogranin A were found to be at higher risk of developing CC [3,4]. Management involves a combination of symptomatic management and use of serotonin receptor inhibitors to directly block hormone effect, utilizing agents such as cyproheptadine and telotristat ethyl [4]. Preventative measures, such as pre-treatment administration of octreotide and correction of nutritional deficiencies have shown efficacy in reducing incidence of CC [4]. Review of our own institutional history of administering lutetium-177-dotatate therapy revealed no incidences of CC, and only one incidence of moderate dyspnea in a patient suffering bronchial carcinoid, which required 1 day hospitalization.

Conclusion: Carcinoid crisis is a rare but potentially life-threatening adverse effect of lutetium-177-dotatate therapy. Prompt recognition and management of this disease is essential to successful intervention and reducing mortality.

References:

1. Modlin IM, Kjell Oberg DC, Jensen R, et al. “Gastroenterohepatic Neuroendocrine Tumors.” *Lancet Oncol*, 2008; 9(1):61-72.
2. Jia AY, Kashani R, Zaorsky NG, et al. “Lutetium-177 DOTATATE: A Practical Review.” *Practl Radiat Oncol*, 2022; 12(4):305-11.
3. Kendi A, Tuba TR, Halfdanarson AP, et al. “Therapy With 177Lu-DOTATATE: Clinical Implementation and Impact on Care of Patients With Neuroendocrine Tumors.” *Am J Roentg*, 2019; 213(2):309-17.
4. de Keizer B, van Aken MO, Feelders RA, et al. “Hormonal crises following receptor radionuclide therapy with the radiolabeled somatostatin analogue [^{177}Lu-DOTA0,Tyr3]octreotate.” *Eur J Nucl Med Mol Imaging,* 2008; 35:749–755.
5. del Olmo-Garcia MI, Muros MA, Lopez-de-la-Torre M, et al. “Prevention and Management of Hormonal Crisis during Theragnosis with LU-DOTA-TATE in Neuroendocrine Tumors. A Systematic Review and Approach Proposal.” *J Clin Med*, 2020; 9(7).

^{68}Ga-DOTATATE PET/MRI-Guided Disease Extent Evaluation and Radiation Treatment Planning in Recurrent Pineal Parenchymal Tumor of Intermediate Differentiation (PPTID)

Jaswal, S., * Zan, E., Castellanos, H. S., * Beal, K., ** Osborne, R. J., * Ivanidze, J. *
*Department of Radiology, Division of Molecular Imaging and Therapeutics, New York Presbyterian Hospital/Weill Cornell Medicine, New York
**Department of Radiation Oncology, New York Presbyterian Hospital/Weill Cornell Medicine, New York

Background:
Pineal Parenchymal Tumor of Intermediate Differentiation (PPTID) is a rare neoplasm arising from pineal parenchymal cells. PPTID are considered WHO grade 2 or 3, and fall in between pineocytoma (well differentiated, WHO grade 1) and pineoblastoma (poorly differentiated, WHO grade 4), with WHO classification determined by histology. On MRI, PPTID demonstrates avid enhancement. Clinical symptoms reflect the mass effect of the tumor on adjacent structures, with compression of the cerebral aqueduct commonly leading to obstructive hydrocephalus and compression of the tectum commonly leading to diplopia and Parinaud syndrome. Surgical resection is the primary form of treatment; postoperatively, radiotherapy is often pursued. In the postoperative setting, MRI has limitations in differentiating postoperative inflammatory enhancement from residual neoplasm. ^{68}Ga-DOTATATE is a PET radiotracer that binds somatostatin receptor 2 (SSTR2) with high avidity and has demonstrated utility in SSTR2-positive brain and skull base tumors such as meningioma and paraganglioma. SSTR2 is also overexpressed in PPTID. We present a patient with PPTID in whom DOTATATE PET/MRI was helpful in disease extent delineation and subsequent clinical management.

Case presentation:
A 58-year-old woman first presented 12 years prior to the current presentation with severe headaches and vomiting and was found to have a calcified heterogeneous pineal mass, for which she underwent subtotal resection and cranio-spinal irradiation (CSI). The patient subsequently was stable with no evidence of recurrence until 2 years prior to this presentation when she experienced progressive gait imbalance. Subsequent brain MRI demonstrated multifocal enhancing lesions suspicious for recurrence, and the patient underwent repeat surgery. Subsequent MRI demonstrated the increased size of residual lesions along the tentorium and suprasellar cistern, suspicious for tumor progression, for which the patient received additional RT. At the time of the current presentation, the patient was referred for confirmation of suspected re-recurrence based on MRI, which demonstrated increased nodular enhancement along the left cerebellar tentorium, narrowing the straight sinus, with discontiguous nodular foci along the floor of the left middle cranial fossa, along the left cerebellar hemispheric convexity, as well as in the suprasellar cistern, suspicious for disease progression. On ^{68}Ga-DOTATATE PET/MRI, the regions of nodular enhancement demonstrated circumscribed moderate avidity, confirming multifocal recurrent SSTR2-positive neoplasm. DOTATATE PET/MRI thus was critical in non-invasively confirming the suspected diagnosis and allowed optimized RT planning for subsequent Gamma knife radiosurgery.

Conclusion:

We present the – to our knowledge –first case of PPTID imaged with DOTATATE PET/MRI, which confirmed the suspected diagnosis of multifocal recurrence and improved tumor extent delineation for subsequent radio-surgical planning.

Images:

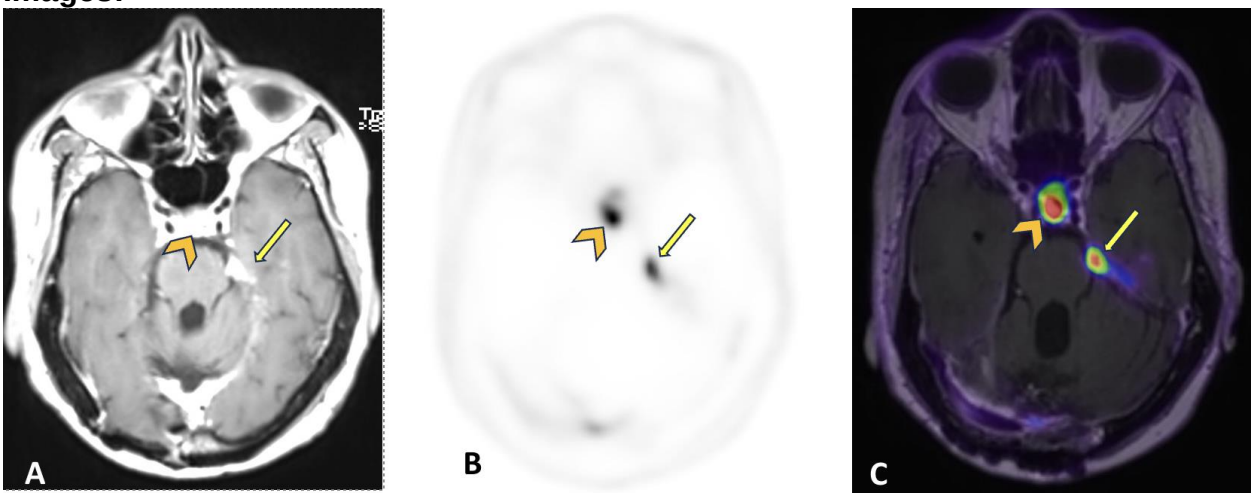

Fig. 1: Dural-based nodular enhancement along the left tentorium visualized on axial postcontrast T1 image **(A)** demonstrates intense DOTATATE avidity with SUV up to 16.0 on PET **(B)** and PET/MRI fused **(C)** images represented by arrows. Arrowhead representing physiologic DOATATE avidity in the pituitary gland.

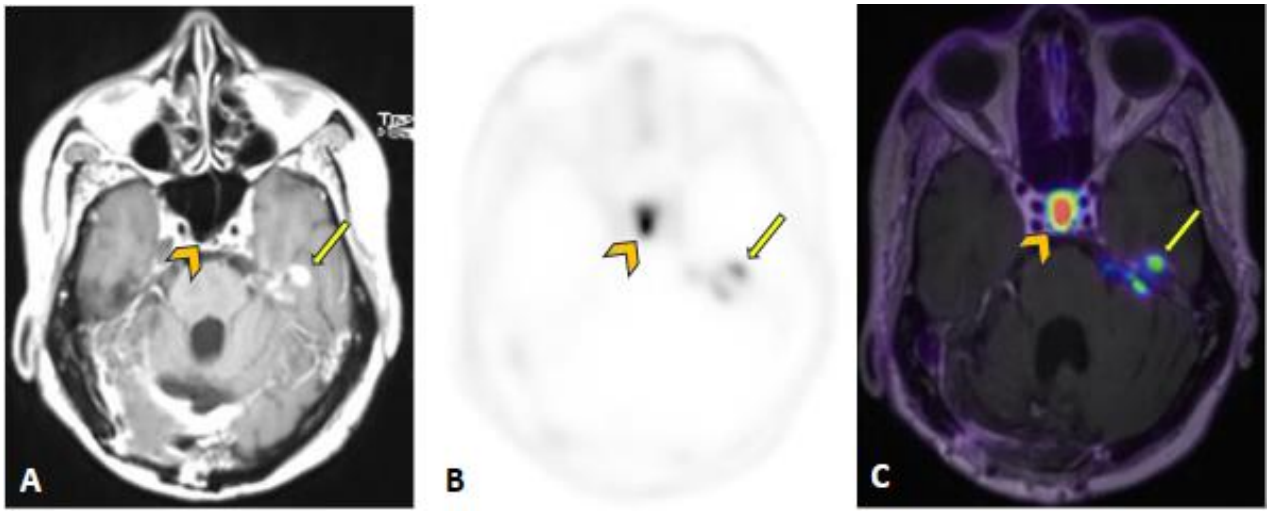

Fig 2: Dural based nodular enhancement along the floor of the left middle cranial fossa, somewhat ill-defined on axial postcontrast T1 **(A)** demonstrates moderate avidity on PET **(B)** and fused PET/MRI images **(C)** represented by arrows. Arrowhead representing physiologic DOATATE avidity in the pituitary gland.

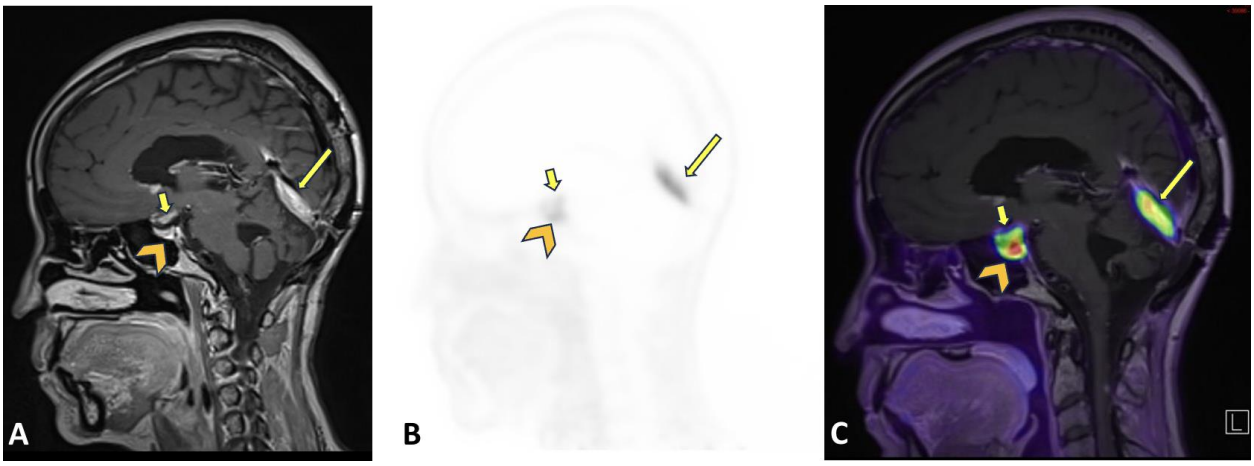

Fig 3: Dural based nodular enhancing mass narrowing the straight sinus (arrow) as visualized on sagittal postcontrast T1 images **(A),** with moderate DOTATATE avidity on PET **(B)** and fused PET/MRI images **(C)**. Arrowhead representing physiologic DOATATE avidity in the pituitary gland, better delineated against suprasellar disease (short arrow) compared to MRI alone.

Spinal Tuberculosis on ^{18}F-FDG Positron Emission Tomography (FDG PET) – a great mimicker of widespread osseous metastatic disease.

Title

Spinal Tuberculosis on ^{18}F-FDG Positron Emission Tomography (FDG PET) – a great mimicker of widespread osseous metastatic disease.

Correspondence

Aspan Meherzad Shokrekhuda

ashokrekhu@montefiore.org

Tel (718) 920-5013 / Fax (718) 920-2629

Montefiore Medical Center and the Albert Einstein College of Medicine

Division of Nuclear Medicine, Department of Radiology

111 E 210Th St

The Bronx, NY, 10467

Authors

Aspan M. Shokrekhuda, MD; Adithya Hari, MD; Deepak Kalbi, MD; Renee Moadel, MD

SNMMI Abstract

Objective:

To bring to the reader's attention that tuberculosis can mimic diffuse FDG avid skeletal metastatic disease.

Background: Positron Emission Tomography (PET) with ^{18}F-FDG is used for staging, evaluating response to treatment, and assessing recurrence in various malignancies. However, an increase in FDG activity is seen in numerous benign etiologies including infections. Tuberculosis (TB), a disease not frequently encountered in the United States, can involve the spine and other osseous structures.

Method: This exhibit will illustrate a case of spinal tuberculosis, which was initially being evaluated as widespread osseous metastatic disease from an unknown primary. The patient's workup included an MRI of the thoracolumbar spine, a technetium-99^{m} methylene diphosphonate bone scintigraphy (MDP bone scan), and an FDG PET scan. The FDG PET study was used to localize the most suitable skeletal biopsy site. The results of this biopsy confirmed the presence of spinal tuberculosis.

Results: A 33-year-old male, who was an active smoker initially presented with complaints of back pain. On his initial MRI of the thoraco-lumbar spine, the patient was found to have multiple enhancing osseous lesions which were suspicious for osseous metastatic disease. A subsequent MDP bone scan visualized multiple foci of moderate uptake in mixed sclerotic and lytic lesions within the thoracolumbar spine. These findings were viewed as suspicious for osseous metastatic disease with an unknown primary.

Thereafter, the patient underwent a FDG PET/CT from the base of the skull to the mid thighs with 8.0mCi of 18^{F}-FDG and imaging 60 minutes postinjection time. The FDG PET/CT demonstrated multiple mixed sclerotic and lytic lesions involving primarily the spine with intense FDG uptake. The SUV max within the osseous lesions was up to 25.7 (the hepatic SUV max was 2.5).

A core needle biopsy was performed of the lesion with the highest SUV max which involved the right superior sacral ala, with the biopsy results indicating non-necrotizing granulomatous inflammation with epithelioid giant cells, which is consistent with tuberculosis.

Summary: In this patient, the intense FDG uptake within numerous osseous lesions was found to be due to widespread skeletal tuberculosis, which is an unusual diagnosis in the United States.

FDG PET/CT helped localize a biopsy site from which a final pathological diagnosis was obtained.

Solely osseous metastatic disease unresponsiveness post ^{177}Lutetium-Dotatate therapy for metastatic well-differentiated gastroenteropancreatic neuroendocrine tumors – is there a role for further nuclear medicine therapy agents?

Title

Solely osseous metastatic disease unresponsiveness post ^{177}Lutetium-Dotatate therapy for metastatic well-differentiated gastroenteropancreatic neuroendocrine tumors – is there a role for further nuclear medicine therapy agents?

Correspondence

Aspan Meherzad Shokrekhuda

ashokrekhu@montefiore.org

Tel (718) 920-5013 / Fax (718) 920-2629

Montefiore Medical Center and the Albert Einstein College of Medicine

Division of Nuclear Medicine, Department of Radiology

111 E 210Th St

The Bronx, NY, 10467

Authors

Aspan M. Shokrekhuda, MD; Rylen Stratford, MD; Deepak Kalbi, MD; Surita Banerjee, MD; Ana Valdivia, MD

SNMMI Abstract

Objective: To explore the pathophysiology and further potential nuclear medicine-based treatment options for unresponsiveness of osseous metastatic lesions, with overall improvement of other metastatic sites (such as lymphadenopathy and soft tissue lesions) after completion of ^{177}Lutetium-Dotatate therapy (LutaThera) for metastatic well-differentiated gastroenteropancreatic neuroendocrine tumors.

Background: Lutathera was the first peptide receptor radionuclide therapy (PRRT) to be approved by the FDA in the USA, due to its effectiveness in improving the overall progression-free survival in patients with progressive, metastatic well differentiated gastroenteropancreatic neuroendocrine tumors. The overall mechanism of action for LutaThera involves its binding to

somatostatin receptors within the primary as well as metastatic tumor sites. One of the main parameters for assessing treatment besides evaluation of the patient's chromogranin levels, involves comparing the pre-treatment and post-treatment ^{68}Gallium-Dotatate Positron Emission Tomography (Dotatate PET scan) with the primary malignancy and metastatic lesions being assigned a Krenning Score based on their SUV Max compared to the liver and spleen SUV max. There are numerous studies about LutaThera therapy in various institutions exploring positive response or progressions of disease. However, there are a dearth of studies exploring mixed response involving solely osseous metastasis progression.

Method: This educational exhibit will review the pathophysiology of well-differentiated gastroenteropancreatic neuroendocrine tumors, and receptor binding of somatostatin analogs to the somatostatin receptors expressed within these tumors. It will present a case of a patient with progressive metastatic well-differentiated gastroenteropancreatic neuroendocrine tumors and the Dotatate PET scan imaging findings prior to initiation of LutaThera therapy. Additionally, the exhibit will review the post therapy follow-up Dotatate PET scan.

Results: A 67-year-old male with metastatic low-grade neuroendocrine tumor with progression on octreotide and poor tolerance to second line treatment with Everolimus, was referred for LutaThera therapy at our institution. The patient had a pretherapy Dotatate scan with 5.9 mCi of ^{68}Gallium-Dotatate and imaging 60 minutes post minutes injection. This pre-therapy Dotatate PET scan visualized innumerable hepatic metastatic lesions with intense uptake (SUV max 44.8, Krenning score 4), prominent lymphadenopathy with intense uptake (SUV max 41.4, Krenning score 4)), and numerous osseous lesions (SUV max 12.2, Krenning score 4)).

Thereafter the patient received 4 cycles of LutaThera doses, which were 8 weeks apart with 200mCi of Lutathera for each dose. There was no imaging follow-up while the patient received

the 4 cycles of LutaThera. Eighty-seven days after the completion of the 4th cycle of LutaThera, the patient underwent a post therapy Dotatate PET scan with 4.7 mCi of ^{68}Gallium-Dotatate and imaging 60 minutes post injection time.

On the post-therapy Dotatate PET scan there was dramatic favorable response in his liver lesions (SUV max of 29.3, Krenning score 4) from previously SUV max 44.8) and lymphadenopathy (SUV max 22.5, Krenning score 4) from previously SUV max, 41.4). However, the osseous lesions remained unresponsive, with persistent intense uptake within his osseous lesions (SUV max 11.5, Krenning score 4).

Summary: LutaThera, a PRRT, is known to show significant improvement in the progression-free survival in patients with well-differentiated gastroenteropancreatic neuroendocrine tumors. The principal disease burden assessment on imaging pre and post therapy is done using a Dotatate PET scan. As per the NETTER-1 trial, the Overall Response Rate (ORR) was into categories including complete response (CR) and partial response (PR). CR was defined as the complete disappearance of all target lesions, while partial response was defined as ≥30% decrease in the sum of diameters of target lesions, taking as reference the baseline sum diameters. Additionally, there has been numerous research exploring partial response post LutaThera. However, there are limited discussions of unresponsive osseous lesions solely and their significance, compared to other lesions. Furthermore, there have been limited discussions for the role of other nuclear medicine-based therapy agents that could potentially target solely widespread osseous lesions along with LutaThera . Additional studies exploring the pathophysiology unresponsiveness of solely osseous based lesions post LutaThera therapy may show potential in improving the treatment structure and further advancement of theranostics.

FDG PET/CT: A Crucial Diagnostic Aid for Endocarditis, Shaping Treatment Strategies

Deepak Kalbi[1], MD; Ghazaleh Mehdipoor[1], MD; Aspan Shokrekhuda[1], MD; and Mark I. Travin[1], MD

1 Department of Radiology, Division of Nuclear Medicine, Montefiore Medical Center/ The university Hospital for Albert Einstein College of Medicine

Background: With a rising incidence of device-related endocarditis, prompt and accurate diagnosis is essential, especially in patients with prosthetic valves. Although transesophageal echocardiography (TEE) is a helpful diagnostic tool for native valve endocarditis, it is often limited in diagnosing. Prosthetic valve endocarditis (PVE). ^{18}F-Fluorodeoxyglucose -positron emission tomography computed tomography (FDG PET/CT) is a valuable tool for early detection and comprehensive assessment of endocarditis, even in its early stages. A few studies have also suggested that FDG PET/CT is superior to radiolabeled WBC based imaging in the diagnosis of cardiovascular infection. According to the 2023 ESC guidelines for the management of endocarditis, suspected PVE is a class IB indication for doing FDG PET/ CT(A) and cardiac CTA to detect valvular lesions and confirm the diagnosis of infective endocarditis.

Methods: We present 3 cases in which FDG PET/CT was used for diagnosis of endocarditis in the setting of various diagnostic complexities. Also included are correlative imaging studies with TEE and low dose CT. For FDG PET/CT, patients are asked to consume a 12 hour high fat low carbohydrate diet followed by 12 hour fasting and 50 IU/kg of heparin is administered 15 minutes prior to testing to limit tracer uptake in healthy myocardium. As per EANM recommendations, the suggested FDG PET/CT administered activity ranges from 2.5-5 MBq/kg with an injection-to-scan time start time interval of 55-75 minutes. Although FDG remains intracellular for 3.5–4 hours post-injection, delaying acquisition to improve diagnostic accuracy in FDG PET/CT is discouraged due to the higher risk of false positives outweighing the marginal sensitivity increase in partial volume effect. When assessing patients with prosthetic valves or cardiac devices, the imaging specialist should examine non-attenuated images in addition to attenuation-corrected images to avoid potential false positives caused by

scatter and beam-hardening artifacts, ensuring accurate diagnosis of suspected prosthetic valve or device infection.

Results: All three patients had bacteremia. However, subsequent evaluation with TEE and tagged white blood cell (WBC) testing yielded negative results. Due to strong clinical suspicion, FDG PET/CT imaging was performed and confirmed the diagnosis of prosthetic valve endocarditis. Appropriate antibiotics were administered, with subsequent negative blood cultures.

Conclusions: FDG PET/CT is an accurate diagnostic tool for early detection and comprehensive evaluation of intramyocardial abscess as well as extracardiac extension of endocarditis in patients with prosthetic valves. Whole body FDG PET/CT imaging is encouraged in the workup for suspected PVE because they help in the detection of septic emboli which are pathognomonic for the diagnosis of endocarditis. This series emphasizes the added value of FDG PET/CT for diagnosing endocarditis when TEE or other diagnostic modalities are inconclusive or negative.

References:

1. Delgado V, Ajmone Marsan N, de Waha S, Bonaros N, Brida M, Burri H, Caselli S, Doenst T, Ederhy S, Erba PA, Foldager D, Fosbøl EL, Kovac J, Mestres CA, Miller OI, Miro JM, Pazdernik M, Pizzi MN, Quintana E, Rasmussen TB, Ristić AD, Rodés-Cabau J, Sionis A, Zühlke LJ, Borger MA; ESC Scientific Document Group. 2023 ESC Guidelines for the management of endocarditis. Eur Heart J. 2023 Oct 14;44(39):3948-4042. doi: 10.1093/eurheartj/ehad193. Erratum in: Eur Heart J. 2023 Sep 20;: PMID: 37622656.
2. Ten Hove D, Slart RHJA, Sinha B, Glaudemans AWJM, Budde RPJ. 18F-FDG PET/CT in Infective Endocarditis: Indications and Approaches for Standardization. Curr Cardiol Rep. 2021 Aug 7;23(9):130. doi: 10.1007/s11886-021-01542-y. PMID: 34363148; PMCID: PMC8346431.
3. Martineau P, Grégoire J, Harel F, Pelletier-Galarneau M. Assessing cardiovascular infection and inflammation with FDG-PET. Am J Nucl Med Mol Imaging. 2021 Feb 15;11(1):46-58. PMID: 33688455; PMCID: PMC7936252.
4. Tarkin JM, Chen W, Dweck MR, Dilsizian V (2023) Molecular Imaging of Valvular Diseases and Cardiac Device Infection. Circ Cardiovasc Imaging 16:e014652
5. Chen W, Sajadi MM, Dilsizian V (2018) Merits of FDG PET/CT and Functional Molecular Imaging Over Anatomic Imaging With Echocardiography and CT Angiography for the Diagnosis of Cardiac Device Infections. JACC Cardiovasc Imaging 11:1679-1691
6. Saeedan MB, Wang TKM, Cremer P et al (2021) Role of Cardiac CT in Infective Endocarditis: Current Evidence, Opportunities, and Challenges. Radiol Cardiothorac Imaging 3:e200378
7. McDermott BP, Mohan S, Thermidor M, Parchuri S, Poulose J, Cunha BA (2004) The lack of diagnostic value of the indium scan in acute bacterial endocarditis. Am J Med 117:621-623

8. Hoey ET, Gulati GS, Ganeshan A, Watkin RW, Simpson H, Sharma S (2011) Cardiovascular MRI for assessment of infectious and inflammatory conditions of the heart. AJR Am J Roentgenol 197:103-112

Diagnosis of Pulmonary Artery Intimal Sarcoma using FDG-PET-CT

Ishaan Khurana, Danielle Barnett MD, Thomas Ng MD, and Bashar Kako MD

Background:

Pulmonary Artery Intimal Sarcoma (PAIS) is a rare disease with a poor prognosis and survival estimates of 11-18 months[,9]. PAIS originates from the intimal layer of the pulmonary trunk, growing eventually to obstruct pulmonary blood flow[3,4]. It clinically presents in a as similar manner as pulmonary embolism, with symptoms of dyspnea, syncope, and hemoptysis. This similar presentation can result in misdiagnosis with patients receiving anti-coagulation instead of anti-neoplastic therapy [7,8,10]. Molecular imaging characterization offers one way to distinguish these disease entities. PAIS can demonstrate intense FDG avidity on PET/CT, while a bland pulmonary embolus (PE) will at most be mildly FDG avid. An additional anatomic feature of PAIS is the wall-eclipsing sign in which the lesion eclipses the pulmonary wall, resulting in a rounded, bulging, or lobulated surface[4,6,9,10]. PAIS is treated with surgery based on the stage, and there has been some success with chemotherapy, but the largest determinant of an improved prognosis remains early and accurate diagnosis[10].

Methods:

The patient is a 70-year-old man who, during a lung cancer screening chest CT was found to have a new 1 cm pulmonary nodule in the right upper lobe. This prompted further work-up with FDG-PET-CT due to the size of the pulmonary nodule. Whole-body PET-CT was conducted, which demonstrated intense radiotracer uptake to the pulmonary nodule concerning for malignancy. However, it also demonstrated an intensely FDG-avid mass in the right pulmonary artery.

Results:

The lung cancer screening CT revealed a new 1 cm pulmonary nodule in the right upper lobe (Figure 1A). Of note, the pulmonary artery lesion was not described on the non-contrast low-dose screening CT, although it can be seen retrospectively as a hypodensity within the pulmonary artery (Figure 1B). The combined FDG-PET- contrast-enhanced diagnostic CT demonstrated an extensive low attenuation filling defect within the main pulmonary artery with extension into the right pulmonary artery. The mass caused expansion of the diameter of the right pulmonary artery and demonstrated heterogeneous internal contrast enhancement (Figure 2B). The mass was intensely FDG avid (Figure 2C). The sagittal reformat demonstrates the “wall eclipsing sign,” in which the lesion infiltrates beyond the pulmonary artery and eclipses the wall of the vessel[3,4]. This contrasts with an acute bland PE, which should not demonstrate internal contrast enhancement and may have, at most, mild FDG uptake. There was also an increase in the size of the right upper lobe nodule to 1.2 cm in approximately two months as well as additional new sub-centimeter subpleural nodules. Due to the intense FDG uptake of the enlarging dominant nodule, the differential consideration was primary lung malignancy versus metastases (Figure 2A). The patient was placed on anticoagulation and, with a poor prognosis, underwent a palliative pulmonary thromboendoarterectomy. Following this, the patient decided to pursue treatment in their home country.

Conclusions:

FDG-PET-CT can be used to differentiate pulmonary artery intimal sarcoma from acute bland pulmonary embolism. The clinical presentation of both PAIS and acute PE are similar and non-specific. However, radiological features, including the anatomic configuration, increased FDG uptake, and internal contrast enhancement, should raise a degree of suspicion about its diagnosis and can differentiate it from bland PE and aid prompt medical treatment.

Images:

1A. Lung Cancer Screening Chest CT: Axial slice through upper lung zones on this low dose non-contrast CT demonstrates a 1 cm pulmonary nodule in the posterior aspect of the left upper lobe.

1B. Lung Cancer Screening Chest CT: Axial slice through pulmonary artery on this low dose non-contrast CT retrospectively demonstrates subtle hypodensity in the main and right pulmonary artery.

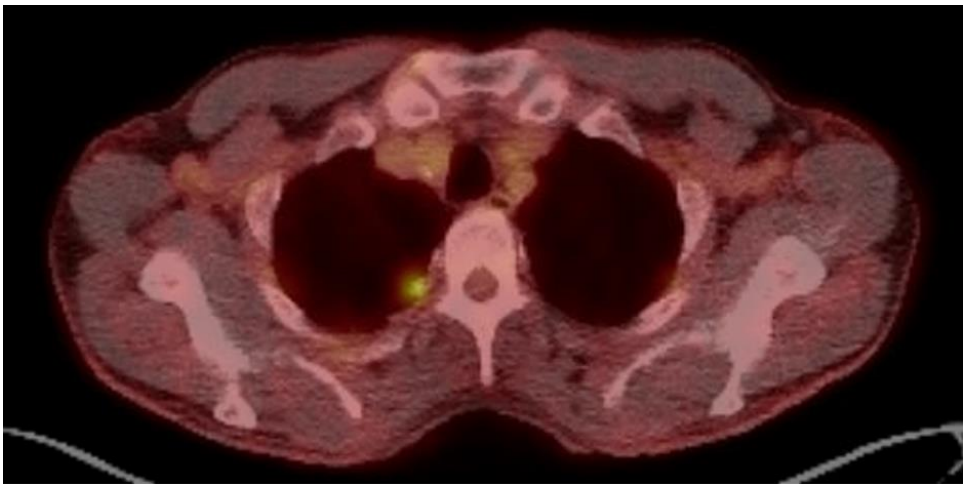

2A. PET/CT: Axial slice through upper lung zones demonstrates intense FDG avidity of pulmonary nodule.

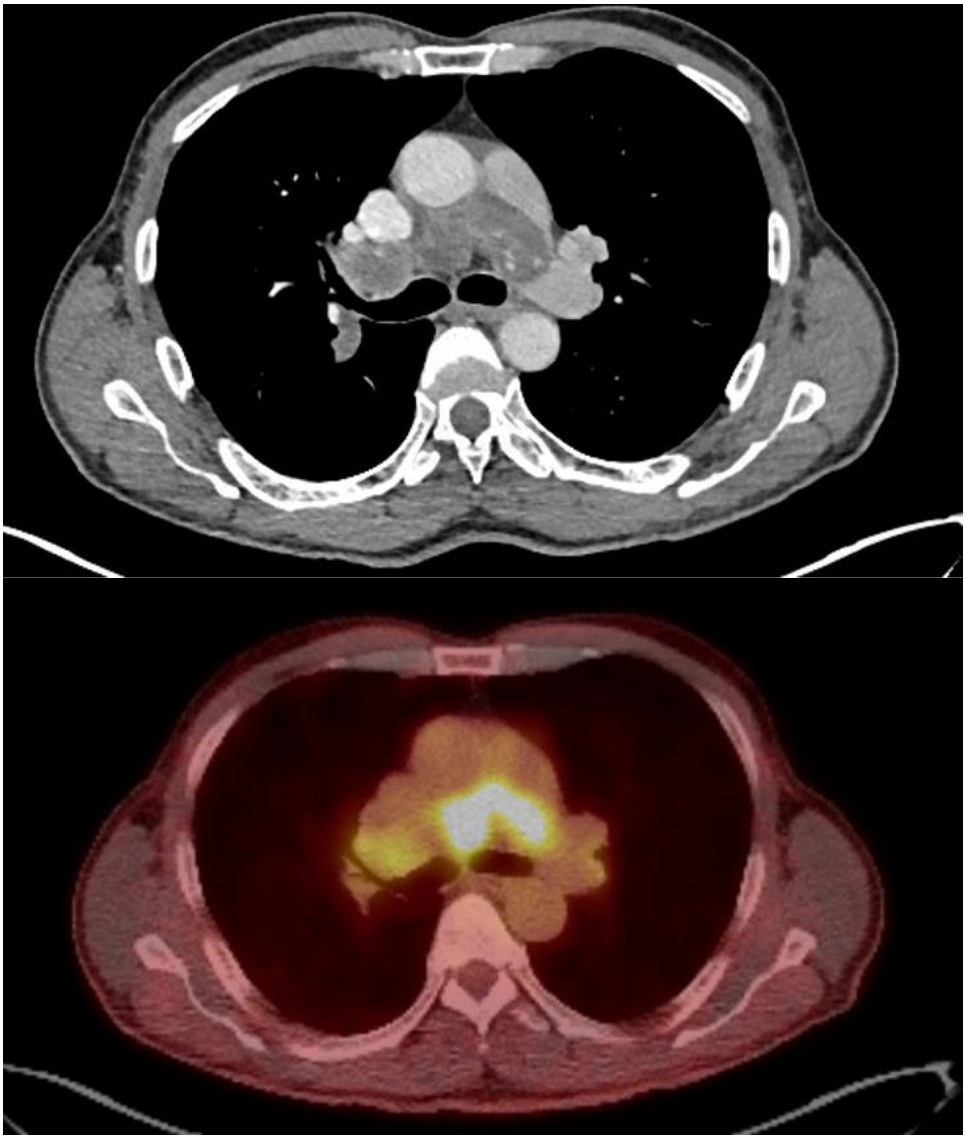

2B/C. PET/CT with corresponding contract enhanced diagnostic chest CT: Axial slice through the pulmonary artery demonstrates a heterogeneous and enhancing mass involving the bifurcation of the main pulmonary artery with extension into the right pulmonary artery. The mass demonstrates intense FDG avidity.

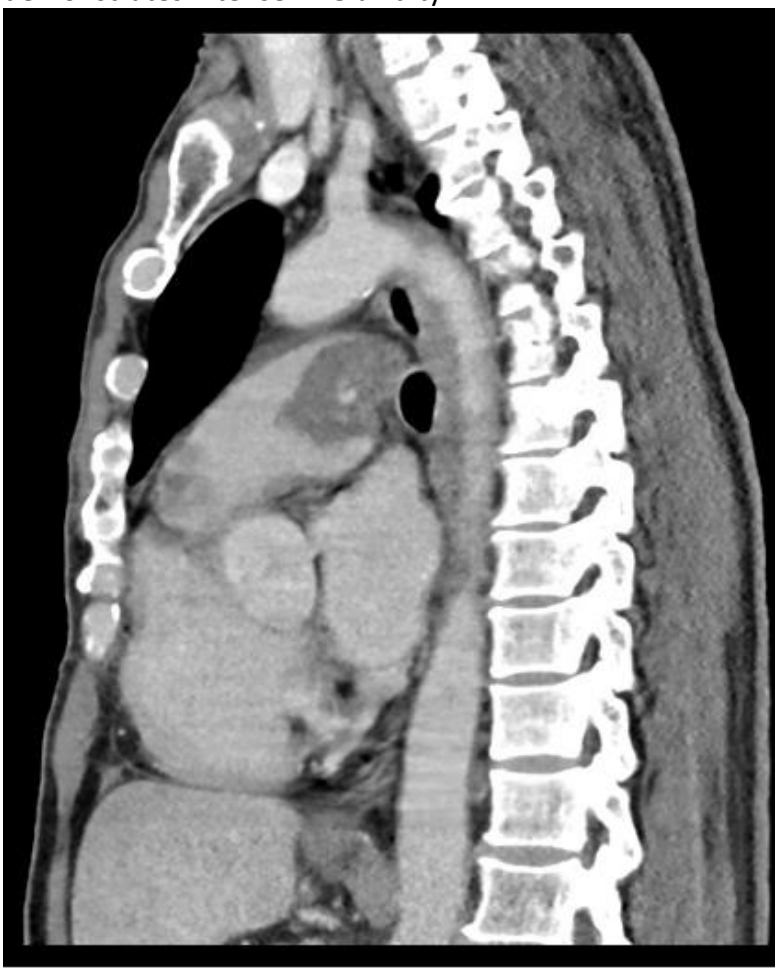

3. Diagnostic Chest CT: Sagittal slice through the main pulmonary artery demonstrates a hypodense mass in the main pulmonary artery which eclipses the posterior wall of the vessel consistent with the “wall eclipsing sign.”

Sources:

1) Attinà, D., Niro, F., Tchouanté, P., Mineo, G., Russo, V., Palazzini, M., Galiè, N., Fanti, S., Lovato, L., & Zompatori, M. (2013). Pulmonary artery intimal sarcoma. Problems in the differential diagnosis. *La Radiologia Medica*, *118*(8), 1259–1268. https://doi.org/10.1007/s11547-013-0943-x
2) Deng, L., Zhu, J., Xu, J., Guo, S., Liu, S., & Song, Y. (2018). Clinical presentation and surgical treatment of primary pulmonary artery sarcoma. *Interactive CardioVascular and Thoracic Surgery*, *26*(2), 243–247. https://doi.org/10.1093/icvts/ivx318
3) *Differential diagnosis and treatment approach to pulmonary artery sarcoma: A case report and literature review | European Respiratory Society*. (n.d.). Retrieved September 26, 2023, from https://openres.ersjournals.com/content/6/3/00124-2020
4) Gan, H.-L., Zhang, J.-Q., Huang, X.-Y., & Yu, W. (2013). The Wall Eclipsing Sign on Pulmonary Artery Computed Tomography Angiography Is Pathognomonic for Pulmonary Artery Sarcoma. *PLoS ONE*, *8*(12), e83200. https://doi.org/10.1371/journal.pone.0083200
5) Halank, M., Jakob, C., Kolditz, M., Hoeffken, G., Kappert, U., Ehninger, G., & Weise, M. (2010). Intimal Pulmonary Artery Sarcoma Presenting as Severe Dyspnea and Right Heart Insufficiency. *Onkologie*, *33*(6), 313–316. https://doi.org/10.1159/000313861
6) Kim, C., Kim, M. Y., Kang, J.-W., Song, J. S., Lee, K. Y., & Kim, S.-S. (2018). Pulmonary Artery Intimal Sarcoma versus Pulmonary Artery Thromboembolism: CT and Clinical Findings. *Korean Journal of Radiology*, *19*(4), 792–802. https://doi.org/10.3348/kjr.2018.19.4.792
7) Lu, P., & Yin, B.-B. (2020). Misdiagnosis of primary intimal sarcoma of the pulmonary artery as chronic pulmonary embolism: A case report. *World Journal of Clinical Cases*, *8*(5), 986–994. https://doi.org/10.12998/wjcc.v8.i5.986
8) Parish, J. M., Rosenow, E. C., Swensen, S. J., & Crotty, T. B. (1996). Pulmonary Artery Sarcoma: Clinical Features. *CHEST*, *110*(6), 1480–1488. https://doi.org/10.1378/chest.110.6.1480
9) Rabbani, M., Hafiz, A., Algadheeb, M., Tugaleva, E., Bergin, M. L., & Ray Guo, L.-R. (2020). Pulmonary Artery Intimal Sarcoma: A Deadly Diagnosis in Disguise. *CJC Open*, *2*(6), 711–715. https://doi.org/10.1016/j.cjco.2020.07.008
10) Tuft, C., Maheepala, K., Raguparan, A., Naeem, A., Lodh, S., & Lindstrom, S. (2022). Pulmonary artery sarcoma: An important mimic of pulmonary embolism—Case reports and literature review. *Respirology Case Reports*, *10*(2), e0897. https://doi.org/10.1002/rcr2.897
11) Suto, H., Suto, M., Inui, Y., & Okamura, A. (2022). Difficulty in Distinguishing Pulmonary Arterial Intimal Sarcoma from Pulmonary Thromboembolism Using FDG PET/CT. *In vivo (Athens, Greece)*, *36*(3), 1519–1522. https://doi.org/10.21873/invivo.12861
12) Ren, J., Li, H., Zhang, Q., Liu, E., Zeng, B., Huang, Y., Wang, L., & Jiang, L. (2022). Clinical utility of ^{18}F-FDG PET/CT imaging in patients with pulmonary artery sarcoma. *EJNMMI research*, *12*(1), 18. https://doi.org/10.1186/s13550-022-00890-2

Title: Right Ventricular Dysfunction Among Patients Undergoing Stress Myocardial Perfusion Imaging

Author: Jiaqiong Wang M.D., Ph.D., Assistant Professor, Division of Nuclear Medicine, Department of Radiology, Temple University Health System, Fox Chase Cancer Center. Email: jiaqiong.wang@tuhs.temple.edu

Abstract:

Background: Right ventricular (RV) dysfunction is an adverse prognostic marker that has been shown to be related to poorer prognosis with increased risk for heart failure and death. Radionuclide stress myocardial perfusion imaging (MPI) plays an important role for evaluating coronary disease and ventricular function. MPI is widely used to assess the left ventricle (LV) wall perfusion and function. RV size and function can be evaluated in the same MPI study.

Methods: In the current study, 2233 patients underwent stress myocardial perfusion scintigraphy with Tc-99m Tetrofosmin from 7/1/2022 to 10/7/2023. Single photon emission computed tomography (SPECT) perfusion images were obtained. In addition to visual inspection of the reconstructed images, quantitative circumferential count profiles for the left ventricle were generated from apical, mid, and basal short axis images. In addition, a gated SPECT study was performed. The normal upper range of the LV end-diastolic volume (LVEDV) is set at 120ml. The RV end-diastolic diameter (RVEDD) and the LV end-diastolic diameter (LVEDD) were evaluated utilizing the short axis images at the base and the maximal distance between the ventricular endocardium and the interventricular septum. The ratio of RV/LV was calculated as RVEDD/LVEDD at the base. The normal RV/LV ratio is approximately 0.6-0.8. The severity of RV dilatation is graded as mild (the RV/LV ratio between 0.8-1.0), moderate (the RV/LV ratio between 1.0-1.4), and severe dilatation (the RV/LV ratio >= 1.5) (REF 1). According to the latest European Society of Cardiology (ESC) guideline, a RV/LV diameter ratio >1.0 is utilized for determining right ventricle dysfunction (REF 2).

Results: Among these 2233 patients, 152 cases demonstrated RV dilatation (n=152) and / or decreased systolic function (n=64). Of the 152 cases of the RV dilation /dysfunction, the following diagnoses may have been the underlying cause of the problem: 136 cases with history of hypertension, 33 cases had pulmonary disease such as COPD or interstitial lung disease, 18 cases with history of cardiomyopathy, 18 cases status post heart transplant, 13 cases of atrial fibrillation, 18 cases with history of pulmonary hypertension (including but not limited to pulmonary embolism), 2 cases with cardiotoxicity secondary to chemotherapy. In these 152 cases with RV dilatation and /or decreased systolic function, 71 patients had abnormal LV wall perfusion, and/or LV dilatation, and/or abnormal wall motion. However, the other 81 patients present with normal LV wall perfusion, normal ventricular size and systolic function, suggesting that RV dysfunction can be independent of LV function.

Conclusions: Right ventricular dysfunction is multifactorial, can be related to cardiovascular disease and pulmonary pathology, or other etiology. Right ventricular dysfunction can be secondary to or independent from LV dysfunction. Radionuclide

stress MPI can be a useful tool in the assessment of RV function in addition to LV function.

Reference

1. Right Ventricular Size and Function. In the book named “Ultrasound for the Generalist: A Guide to Point of Care Imaging”. https://www.generalistultrasound.com/accreditation/acce/right-ventricular-size-and-function/

2. Konstantinides SV, Meyer G, Becattini C, Bueno H, Geersing GJ, Harjola VP, et al.; ESC Scientific Document Group. 2019 ESC Guidelines for the diagnosis and management of acute pulmonary embolism developed in collaboration with the European Respiratory Society (ERS). Eur Heart J 2020; 41:543–603.

The potential cases to be in the poster:

Case 1. A 59-year-old male with history of IPF s/p double lung transplant and PFO closure (6/15/2017). The patient got COVID-19 pneumonia and complicated by multiple subsegmental PEs (2/9/2022). The patient developed a RUL nodule and the biopsy in 6/2023 revealed positive for mixed squamous cell and small cell carcinoma.

The stress myocardial perfusion test in 7/2023 showed that RV was moderately dilated with hypokinesia. Normal myocardial perfusion with no evidence of scar or ischemia. LV size and function were normal. Calculated LVEF = 60%

Case 2. A 32-year-old female s/p orthotopic heart transplantation (OHT) on 9/16/2017, complicated by AMR and LV dysfunction, LVEF now 40-45%, more recently recurrent and persistent volume overload, with most recent hospitalization in December of 2022 with congestive heart failure, complicated by complete heart block now s/p PPM, complicated by multiple episodes of rejection, allograft dysfunction, and now with a restrictive cardiomyopathy and preserved LVEF. Past surgical history that includes LVAD (7/2/2009); AICD insertion; LVAD (05/04/2016); OHT 9/16/17.

Stress MPI on 8/14/2023 showed moderate RV dilatation with very severe RV hypokinesis. No ischemia or scar. Normal LV size with normal LV wall motion. Calculated LVEF of 63%.

MAG-3 Renography Utilizing SPECT–CT to Diagnose Ureterocolic Fistula

Authors: Affaf Gul, MD; Deepak Kalbi, MD; Rene Moadel, MD.
Department of Radiology, Division of Nuclear Medicine, Montefiore Medical Center/ The university Hospital for Albert Einstein College of Medicine

Background:
Ureterocolic fistula, an uncommon connection between the ureter and the large intestine, is a rare condition [1] and can result from various causes, including iatrogenic factors, spontaneous occurrences, and underlying pathologies such as ureteric calculi, diverticulitis-induced abscess, radiation therapy, or neoplastic processes [2]. Symptoms often include fecaluria, pneumaturia, and recurring urinary tract infections. Traditional diagnostic methods such as X-rays after a barium enema and retrograde cystourethrography, are commonly used to identify ureterocolic fistulas and CT scan is the most sensitive for detecting pneumaturia and fistulous tracts [3].
In this case report, we demonstrate the role of MAG-3 study with a single-photon emission computed tomography/computed tomography (SPECT/CT) in diagnosing pathologies such as ureterocolic or vesicocolic fistulas. Renal scans, employing radiopharmaceuticals with significant renal clearance such as MAG-3, are safe and easily accessible examinations that provide insights into both kidney structure and function.[5] Additionally, they can help clarify anatomical abnormalities leading to renal vascular or urinary tract dysfunction. Dynamic renal scintigraphy, in combination with abdominal SPECT/CT, offers the dual advantage of providing both functional and anatomical imaging during a single session.
Methods:
In this case study, MAG-3 study was used to evaluate a patient with obstructive uropathy. Dynamic renography was performed in the posterior projection and posterior kidney images were obtained using dynamic blood flow imaging for 30 minutes; at different intervals and Lasix was given at 15 minutes into the acquisition. Post-void images, differential function, delayed images and abdominal SPECT/CT were also obtained at 24 hours. A right proximal ureterocolic fistula was detected on scintigraphy , which was confirmed by CT and MRI of the pelvis. This was a rare case of ureterocolic fistula diagnosed by MAG-3 scintigraphy.
Results: A 54-year-old woman with a history of obstructive uropathy due to a bladder mass and persistent hydroureteronephrosis after ureteral stent placement presented with diarrhea one month after stent placement. Due to acute kidney injury (AKI), a noncontrast CT was performed, revealing bilateral nephroureteral stents, severe bilateral hydronephrosis and moderate hydroureter. Also seen was contracted trabeculated thickwalled urinary bladder and liquid stool throughout the colon. The patient underwent MAG-3 study, which displayed urinary radiopharmaceuticals activity in the ascending colon adjacent to the right ureter indicating consistent with a the presence of a fistula. A delayed Delayed planar image and SPECT/CT imaging was acquired at 24 hours post injection which demonstrated activity throughout the colon again confirming the presence of a ureterocolic fistula.
Conclusion: The diagnosis of ureterocolic fistulae can be achieved through urological or gastrointestinal imaging techniques. Excretory urography, retrograde pyelography, and contrast-enhanced CT scans are the most commonly utilized procedures in suspected cases, with antegrade or retrograde ureterography being the most sensitive modality. [6]. In this case, where CT contrast use was precluded due to reduced renal function, the MAG-3 renogram was successfully used to identify and localize the presence of the fistula. Additionally, dynamic renal scintigraphy proves to be a valuable adjunct for not only determining the anatomical location of the pathology but also quantifying renal function and the amount of urine traversing via the fistula, thereby aiding in management and treatment planning.
References:
[1] Almerie M. Q., Culverwell A., Gill J., Harrison J. D. Spontaneous right-sided ureterocolic fistula: a rare complication of colonic diverticular disease. BMJ Case

Reports. 2015;2015 doi: 10.1136/bcr-2015-211282. [PMC free article] [PubMed] [CrossRef] [Google Scholar]
[2] Cirocco WC, Priolo SR, Golub RW. Spontaneous ureterocolic fistula: a rare complication of colonic diverticular disease. Am Surg 1994;60:832–5
[3]Noordzij JW, Garibyan H, Kurth KH. Ureterocolic fistula. Eur Urol 1991;19:85-86.
[4] Conde Santos G, Griñó Garreta J, Bielsa Gali O, et al. Uretero-colonic fistula in nonfunctioning ureter. Arch Esp Urol. 2001;54:1126–1129. [PubMed] [Google Scholar]
[5]Sfakianakis, George N., and Mike F. Georgiou. "MAG3 SPECT: a rapid procedure to evaluate the renal parenchyma." Journal of Nuclear Medicine 38.3 (1997): 478-483.
[6]Ferrie, B. G,: Ureterocolic fistula diagnosed by antegrade pyelography. Urol. Rad., 7: 116, 1985.

Challenging the Conventional: A Hot Nodule Unveiling Thyroid Malignancy

Deepak Kalbi, MD; Aspan Shokrekhuda, MD; Renee Moadel, MD.
Department of Radiology, Division of Nuclear Medicine, Montefiore Medical Center/
The university Hospital for Albert Einstein College of Medicine

Background:

The general population exhibits a significant occurrence of thyroid nodules, with up to a 60% prevalence confirmed by high-resolution ultrasound, of which only a small fraction are malignant [1]. The prevalence of palpable thyroid nodules is approximately 5% in women and 1% in men in iodine-sufficient regions of the world [2]. The clinical importance of thyroid nodules stems from the fact that they could be malignant, which occurs in 7%-15% of cases depending on factors like age, sex, radiation exposure history, family history, etc [3]. High-resolution ultrasound is instrumental in the detection of thyroid nodules in 19%-68% of randomly selected individuals, with higher detection rates in the women and the elderly [4]. Among those patients who are sent for nuclear medicine thyroid scans approximately 80-85% are hypofunctioning or"cold", and about 10% are malignant. Additionally, about 10% of thyroid nodules are hyperfunctioning or "hot", and less than 1% of these are malignant [5].

Methods:

We are presenting an unusual case where a hyperfunctioning "hot" thyroid nodule was found to be malignant. Nuclear medicine thyroid uptake and scan with SPECT/CT imaging was performed 24 Hours following with I-123 sodium iodide as the radiopharmaceutical. A low-energy collimator was used for imaging.

Results:

A 51-year-old female with a past medical history of multinodular goiter and subclinical hypothyroidism presented to the endocrinology clinic. Thyroid ultrasound showed solid nodules within both thyroid lobes measuring up to 3.9 x 2.7 x 3.4 cm on the right and 4.8 x 3.6 x 3.4 cm on the left and the patient underwent a biopsy of multiple nodules which revealed benign pathology on the right and a Bethesda III [7] on the left. After one year, the right nodule measured 5.3 cm X 2.6 cm X 4.4 cm with both solid and cystic parts and was hyperemic. The left nodule was stable, solid, hypoechoic with calcifications and measured 2.2 X 2.2 X 2.4 cm. Six months later, the patient underwent a nuclear thyroid scan which demonstrated a hyperfunctioning or 'hot' thyroid nodule on the right and with suppression of the remaining thyroid tissue. The uptake pattern appeared intense peripherally with central photopenia on SPECT CT, resembling an Owl's eye appearance, indicating central necrosis. While the patient was on Methimazole, her TSH levels eventually normalized, and surgery was recommended but declined by the patient. The patient again underwent an ultrasound one year later, which showed the right thyroid nodule had enlarged further measuring 6.7 x 4.3 x 5.3 cm and the left lobe nodule was 1.9 x 1.2 cm. Repeat biopsy of the right thyroid nodule

showed Bethesda III [7] classification and Thyroseq [8] testing was performed (multigene genomic classifier genetic testing) and came back positive for Phosphatase and tensin homolog (PTEN) and Telomerase reverse transcriptase (TERT) mutations. Four months later, she underwent a total thyroidectomy and pathology revealed a well-differentiated high-grade thyroid carcinoma measuring 7.5 x 5.5 x 5 cm, with >5 mitoses/mm2, tumor necrosis, and extensive angioinvasion. The left thyroid nodule was a 1.6 cm non-invasive follicular thyroid neoplasm (NIFTP). Post thyroidectomy labs showed thyroglobulin level of 64.8 ng/ml and TSH 3.18 uU/mL. Four months later, the patient was referred for radioiodine therapy. Pretherapy whole body scan 4 hours following the oral administration of 400 uCi of I-123 NaI showed remnant uptake in anterior neck and no evidence of metastatic disease. The 4 hours uptake in thyroid bed was 2.4%. The patient received the 154 mCi of iodine-131, and the post-therapy scan confirmed the successful targeting of the thyroid remnant in the neck. Four months later the thyroglobulin level decreased significantly to 0.1ng/mL and TSH level of 3.38 uU/mL.

Conclusion: This case serves as a testament to the fact that hyperfunctioning "hot" thyroid nodules may be associated with underlying malignancy, especially in the presence of the owl's eye sign. Existing literature supports that thyroid nodules with Owl's eye are benign but, in our case, it was malignant which makes it a unique case [6]. This report stresses the importance of considering malignancy as a differential when Owl's sign is present and also the significance of close monitoring and a comprehensive differential diagnosis to ensure timely and appropriate management in similar cases.

References

1. Grani G, Sponziello M, Pecce V, Ramundo V, Durante C. Contemporary Thyroid Nodule Evaluation and Management. J Clin Endocrinol Metab. 2020 Sep 1;105(9):2869–83. doi: 10.1210/clinem/dgaa322. PMID: 32491169; PMCID: PMC7365695.
2. Tunbridge WM, Evered DC, Hall R, Appleton D, Brewis M, Clark F, Evans JG, Young E, Bird T, Smith PA. The spectrum of thyroid disease in a community: the Whickham survey. Clin Endocrinol (Oxf). 1977 Dec;7(6):481-93. doi: 10.1111/j.1365-2265.1977.tb01340.x. PMID: 598014.
3. Hegedüs L. Clinical practice. The thyroid nodule. N Engl J Med. 2004 Oct 21;351(17):1764-71. doi: 10.1056/NEJMcp031436. PMID: 15496625.
4. Guth S, Theune U, Aberle J, Galach A, Bamberger CM. Very high prevalence of thyroid nodules detected by high frequency (13 MHz) ultrasound examination. Eur J Clin Invest. 2009 Aug;39(8):699-706. doi: 10.1111/j.1365-2362.2009.02162.x. PMID: 19601965.

5. Bomeli SR, LeBeau SO, Ferris RL. Evaluation of a thyroid nodule. Otolaryngol Clin North Am. 2010 Apr;43(2):229-38, vii. doi: 10.1016/j.otc.2010.01.002. PMID: 20510711; PMCID: PMC2879398.
6. Ravel R. "Owl eye" sign in thyroid nodule of papillary carcinoma: case report. J Nucl Med. 1976 Nov;17(11):985. PMID: 978261.
7. Ali SZ, Baloch ZW, Cochand-Priollet B, Schmitt FC, Vielh P, VanderLaan PA. The 2023 Bethesda System for Reporting Thyroid Cytopathology. Thyroid. 2023 Sep;33(9):1039-1044. doi: 10.1089/thy.2023.0141. Epub 2023 Jul 8. PMID: 37427847.
8. Desai D, Lepe M, Baloch ZW, Mandel SJ. ThyroSeq v3 for Bethesda III and IV: An institutional experience. Cancer Cytopathol. 2021 Feb;129(2):164-170. doi: 10.1002/cncy.22362. Epub 2020 Oct 8. PMID: 33030808.

Title: ^{177}Lu-PSMA-617-Therapy of a Chemotherapy-Naïve Patient with Metastatic Castration-Resistant Prostate Cancer: A Case Report

Alam, AK., Kulkarni, R., Akinlusi, R., Abdelrahman, A., Cangut, B., Ghesani, M., and Ghesani, NV.

Division of Nuclear Medicine, Department of Diagnostic, Interventional and Molecular Radiology Icahn School of Medicine at Mount Sinai, New York, NY

Background:
The patient is a 71-year-old male who was diagnosed with prostate cancer in 2012 with a prostate specific antigen (PSA) level of 10 ng/mL, Gleason score of 7 (4 +3), stage pT3aN0, and underwent prostatectomy at that time. He subsequently developed several biochemical recurrences with osseous and soft tissue metastases. He was ineffectively treated with intensity-modulated radiation therapy to the prostate bed (2014), multiple androgen-deprivation therapies, as well as radiation therapy to the shoulder and spine, (2017). Fluorine 18 2-(3-{1-carboxy-5-[(6-18F]fluoro-pyridine-3-carbonyl)-amino]-pentyl}-ureido)-pentanedioic acid (^{18}FDCFPyL) PET/CT scan was performed in October 2021, which revealed prostate-specific membrane antigen (PSMA) avid lymph node metastases in the chest, abdomen, and pelvis, consistent with metastatic castration-resistant prostate cancer (mCRPC). For example, PSMA-avid right retrocrural (1.2 cm, SUV max 168) and left supraclavicular (0.7 cm, SUV max 33) lymph nodes were visualized. PSA at the time of the PET/CT scan was 5.47 ng/mL while on darolutamide and androgen-deprivation therapy. Given the patient's history of ischemic and hemorrhagic strokes, he was not a good candidate for chemotherapy and was thus referred by his oncologist for radioligand therapy (RLT) with ^{177}Lu-PSMA-617, a novel, promising option shown to prolong survival in patients with mCRPC.[1] In this report, we will present this patient's subsequent treatment course post ^{177}Lu-PSMA-617 therapy.

Methods:
Following IRB approval, authorization was obtained from the FDA for ^{177}Lu-PSMA-617 therapy for this patient as he was chemotherapy-naïve and thus not eligible to participate in the expanded access program. He was scheduled for a cycle of 6 treatments of 200 mCi of ^{177}Lu-PSMA-617 every 6 weeks. Following each treatment, he underwent same-day tumor imaging scans and was monitored for side effects. Routine labs, including PSA levels, were checked approximately every 2 weeks, including prior to each treatment. To evaluate for RLT response, the patient was scheduled for a post-therapy ^{18}FDCFPyL PET/CT scan. Tumor volumes were measured using the MIM Software® v7.1.7 Segment Lesions research workflow along with PET Edge and Edge+ segmentation methods based on active contouring algorithms.

Results:
The patient received 4 treatments of ^{177}Lu-PSMA-617 on 1/27/2022, 3/10/2022, 7/6/2022, and 8/17/2022 and underwent post-therapy scans (Figure 1). Third and fourth treatments were delayed secondary to sponsor production issues, and thus, the patient additionally underwent a midcycle ^{18}FDCFPyL PET/CT scan. During this time, his PSA levels consistently down-trended from 6.73ng/mL to <0.02ng/mL (Table 1). Pre-therapy, midcycle, and post-therapy ^{18}FDCFPyL PET/CT scans (Figure 2) showed reduction in tumor volume and radiotracer avidity (Table 2).

Further treatment cycles were not given as his PSA levels were undetectable and his tumor volume was reduced by 99.5% after the fourth cycle (Table 2). In June 2023, during a follow-up visit, the patient felt well overall with undetectable PSA levels and no evidence of hematologic or metabolic toxicity 10 months post-therapy.

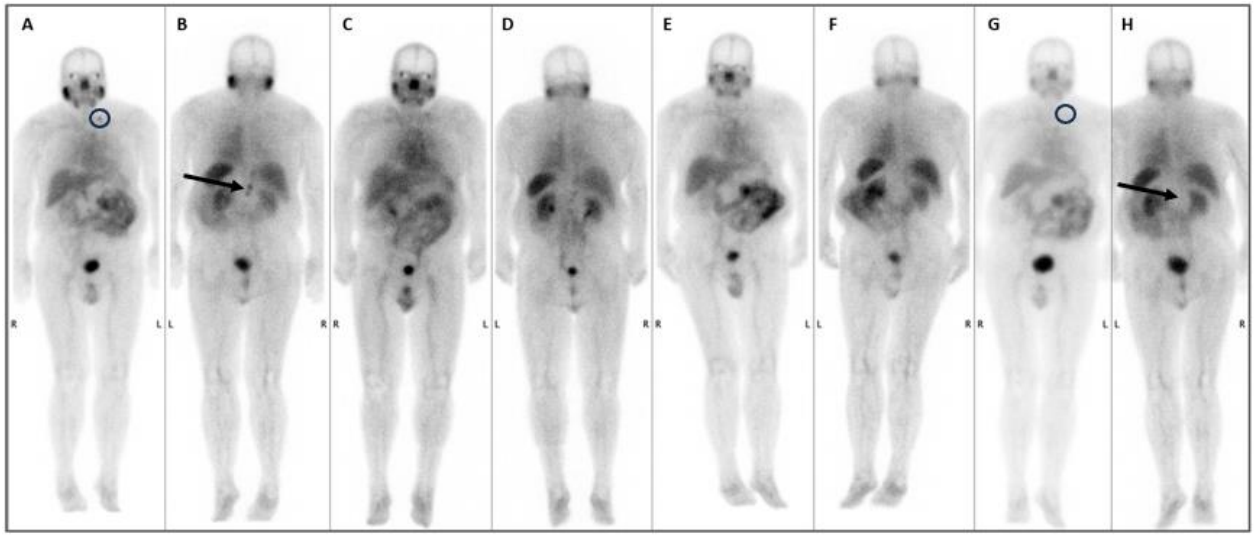

FIGURE 1: 71-year-old male with mCRPC underwent four ^{177}Lu-PSMA-617 treatments on 1/27/2022, 3/10/2022, 7/6/2022, and 8/17/2022. Anterior (A, C, E, G) and posterior (B, D, F, H) images from the post-therapy scans, in order, are seen. Resolution of left supraclavicular (circles) and right retrocrural (arrows) lymph nodes can be seen from the first to fourth post-therapy scan.

12/29/21	1/27/22	2/9/22	3/10/22	3/23/22	5/2/22	5/25/22	6/2/22	6/30/22	7/27/22	8/17/22	8/31/22
5.82 (H)	6.73 (H)	4.27 (H)	2.30	0.95	0.18	0.09	0.07	0.04	0.02	<0.02	<0.02

TABLE 1: Decreasing PSA levels, in ng/mL, are seen with ^{177}Lu-PSMA-617 therapy, which began on 1/27/22 and ended on 8/17/22.

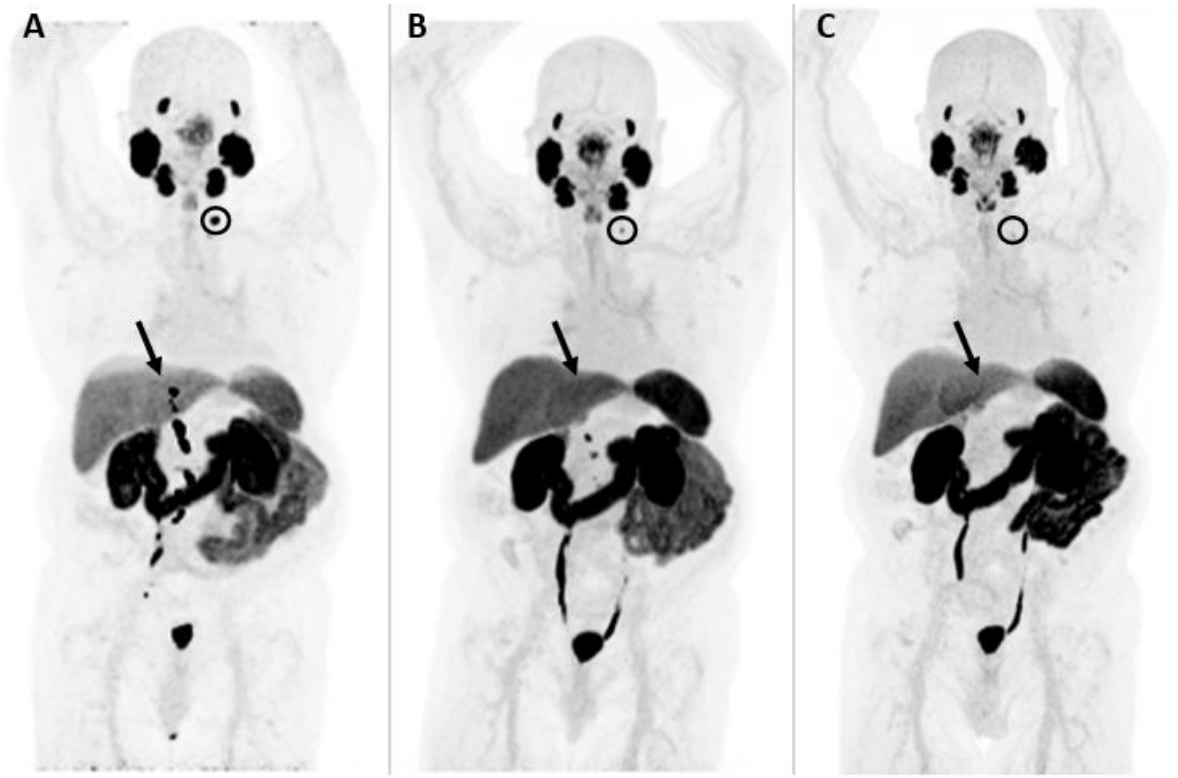

FIGURE 2: MIP images of pre-therapy (A), midcycle (B), and post-therapy (C) ^{18}FDCFPyL PET/CT scans show left supraclavicular (circle) lymph node (pretherapy: 1.2 cm with SUV max 186; posttherapy: 0.7 cm with SUV max 3.7) as well as a right retrocrural (arrow) lymph (pretherapy: 0.7 cm with SUV max 33; posttherapy: 0.4 cm with SUV max 7.2).

Tumor Burden Summary	2021-10-28	2022-06-02		2022-09-23	
	SUVbw	SUVbw	Δ (%)	SUVbw	Δ (%)
Uptake Time (hr)	1.8	1.1	*-39.1*	1.1	*-38.6*
Volume (ml)	14.9	2.2	*-85.1*	0.1	*-99.2*
Max	220	13.1	*-94*	3.7	*-98.3*
Mean	30.1	4.1	*-86.5*	3	*-90.1*
TLA (mean*ml)	447.3	9	*-98*	0.4	*-99.9*

TABLE 2: Decreasing tumor burden seen on pre-therapy (10/28/2021), midcycle (6/2/2022), and post-therapy (9/23/2022) ^{18}FDCFPyL PET/CT scans with ^{177}Lu-PSMA-617 therapy.

Conclusions:

This case demonstrates how ^{177}Lu-PSMA-617 therapy may lead to favorable outcomes in patients with prostate carcinoma, particularly those with small volume soft tissue metastases who are chemotherapy naïve. Further investigations studying a large cohort of these patients with ^{177}Lu-PSMA-617 treatment prior to chemotherapy are needed.

References:

1. Sartor O, de Bono J, Chi KN, Fizazi K, Herrmann K, Rahbar K, Tagawa ST, Nordquist LT, Vaishampayan N, El-Haddad G, Park CH, Beer TM, Armour A, Perez-Contreras WJ, DeSilvio M, Kpamegan E, Gericke G, Messmann RA, Morris MJ, Krause BJ; VISION Investigators. Lutetium-177-PSMA-617 for Metastatic Castration-Resistant Prostate Cancer. N Engl J Med. 2021 Sep 16;385(12):1091-1103. doi: 10.1056/NEJMoa2107322. Epub 2021 Jun 23.